Numerical solution of the nonlinear evolution equation at small x with impact parameter and beyond the leading logarithmic approximation

Jeffrey Berger[1,*] and Anna M. Staśto[1,2,3,†]

[1]*Penn State University, Physics Department, University Park, Pennsylvania 16802, USA*
[2]*RIKEN Center, Brookhaven National Laboratory, Upton, New York 11973, USA*
[3]*Institute of Nuclear Physics, Polish Academy of Sciences, Cracow, Poland*

(Received 14 October 2010; published 11 February 2011)

The nonlinear evolution equation at small x with impact parameter dependence is analyzed numerically. The saturation scales and the radius of expansion in the impact parameter are extracted as functions of rapidity. Running coupling is included in this evolution, and it is found that the solution is sensitive to the infrared regularization. Kinematical effects beyond the leading logarithmic approximation are taken partially into account by modifying the kernel which includes the rapidity-dependent cuts. These effects are important for the nonlinear evolution with the impact parameter dependence.

DOI: 10.1103/PhysRevD.83.034015 PACS numbers: 12.38.−t, 12.38.Bx

I. INTRODUCTION

The high energy limit in quantum chromodynamics is one of the most intriguing problems in strong interaction physics. Since the Large Hadron Collider has recently opened a new kinematic regime, it is of vital importance to understand how one can calculate the cross section at high energies from basic principles in QCD. The Balitsky-Fadin-Kuraev-Lipatov (BFKL) equation obtained in the Regge limit of QCD [1–4] predicted fast growth of the cross section with the energy, due to the exchange of the hard Pomeron. This behavior is, however, known to violate the unitarity bound of the scattering amplitude. Higher order corrections to the BFKL [5–13] tame the growth, but other terms due to the parton recombination [14] and multiple Pomeron exchanges have to be taken into account in order to guarantee the unitarity of the scattering amplitudes.

The Balitsky-Kovchegov equation was derived in [15,16] in the dipole approach [17] to high energy scattering in QCD and independently in the formalism for the operator product expansion at high energy as an evolution of the Wilson line correlators with respect to the rapidity [18–22]. This equation also emerges in the color glass condensate formalism as a limit of the Jalilian-Marian–Iancu–McLerran–Weigert–Leonidov–Kovner functional equation [23–27]; see also [28,29]. The Balitsky-Kovchegov (BK) equation was shown to agree with the BFKL evolution with the triple Pomeron vertex [30,31] when the latter one is restricted to the Möbius space of functions [32] and in the large N_c limit.

Numerous analyses of the BK equation which were performed up to date—see, for example, [33–39]—focused on finding the solutions to this equation under the assumption that the amplitude does not depend on the impact parameter but only on the dipole size and rapidity. This assumption makes the equation relatively easy to solve (at least numerically). Usually one is justifying this approximation by considering the scattering off a very large target, therefore bringing a large scale into the problem. This results in breaking the symmetry between the infrared and ultraviolet regions even in the case of the fixed coupling by generating a saturation scale which acts as a boundary and suppresses the diffusion into the infrared region [35,40,41]. In the momentum space this approximation is equivalent to taking the forward limit in the evolution with the simplifying approximation on the triple Pomeron vertex resulting in zero momentum transfer through the vertex in both Reggeized gluon pairs [42]. On the other hand, the kernel of the equation has the property that it is invariant with respect to the translations, dilatations, rotations, and inversions, which are Möbius transformations. Therefore the solutions to the nonlinear equation should also reflect these symmetry properties, at least in the leading logarithmic, fixed coupling limit. On a deeper level it is related to the Möbius invariance of the $2 \to 4$ Reggeized gluon transition vertex which was demonstrated explicitly [43]. In relation to the experiment, detailed knowledge about the dynamics and expansion in the impact parameter is of the utmost importance for the qualitative and quantitative description of the multiparticle production in hadronic collisions.

In this paper we analyze this equation numerically including the full impact parameter dependence. This is an extension of the previous work [44] where this type of analysis was performed; see also [45]. We significantly improve over Ref. [44] the numerical accuracy and technique which enables us to evolve the equation much faster and to very high values of rapidity, of the order of ~ 50. In this way one can more accurately extract the asymptotic values of different exponents which govern the growth of the saturation scales in this equation. We confirm the results of [44] on the dependence of the scattering

*jxb1024@psu.edu
†astasto@phys.psu.edu

amplitude as a function of dipole size and demonstrate that it vanishes for large dipole sizes. We also find the fast diffusion of the solution in impact parameter space and recover the power tails. The saturation scale for both small and large dipoles is extracted, and the dependencies on the impact parameter and rapidity are found. The results of the solutions to the equation in the leading logarithmic approximation (LL) are compared with the modified version of the equation proposed in [46]. The modified version contains the cutoffs in rapidity which originate from kinematical constraints. These cutoffs contain kinematical constraints in an only approximate way, but we know from the analysis of forward BFKL in momentum space that these constraints are known to reduce the speed of the evolution in a significant way [47]. (For a related analysis on impact parameter dependence in the nonlinear equation and the energy conservation see [48]. The BK without impact parameter dependence and with rapidity cutoffs was also analyzed in [35,49].) We also include the running coupling in our analysis and find that the effect of the running coupling is quite different than in the case without the impact parameter. In this paper we consider a prescription for the running coupling with the external dipole as the scale as well as the prescription derived in [50]. The impact parameter dependent equation is extremely sensitive to the large dipole sizes, and this is the region where the running coupling is very large and needs to be regularized by some other mechanism.

In this analysis we did not attempt to regularize the large dipole size region in any way. It is at present totally unclear how confinement effects should be consistently included in the dipole formalism. Of course, for any phenomenological applications such a cut should be included, perhaps similarly to what was done in [51]. As we were interested in general properties of the evolution we did not attempt here to introduce additional cuts on large dipole sizes (via masses), which would interfere with the specific dynamics of the evolution.

The paper is organized in the following way. In Sec. II we briefly present the BK equation and discuss the modified version which includes the cutoffs in rapidity. In Sec. III we describe the numerical methods of finding the solution. In Sec. IV we first show the results of the solution without the impact parameter and extract the saturation scale for both the LL and the modified equation. In Sec. V we present the solutions with the impact parameter. We discuss the form of the amplitude as a function of the dipole size, extract the saturation scales (for both small and large dipoles), and discuss the form of the impact parameter profile which emerges in the evolution. We present the solutions both in the case of the LL and for the modified kernel. Using the representation in terms of the conformal eigenfunctions we discuss the origins of different peaks in the amplitude as well as present estimates for the rapidity dependence of the small and large dipole saturation scales and the expansion radius in the impact parameter. We also present the estimate of the cross section of the black disk radius and its dependence on the rapidity. In Sec. VI we discuss the results with the running coupling, both for the case without and with impact parameter dependence and for two different prescriptions of the running coupling. Finally, in Sec. VII we state our conclusions.

II. THE BK KERNEL IN LO AND BEYOND

In the leading logarithmic approximation in $\ln 1/x$, the nonlinear Balitsky-Kovchegov [15,16,18–22] evolution equation derived in the dipole picture [17] has the following form:

$$\frac{\partial N_{\mathbf{x}_0\mathbf{x}_1}}{\partial Y} = \bar{\alpha}_s \int \frac{d^2\mathbf{x}_2}{2\pi} \frac{(\mathbf{x}_0-\mathbf{x}_1)^2}{(\mathbf{x}_0-\mathbf{x}_2)^2(\mathbf{x}_1-\mathbf{x}_2)^2} \times [N_{\mathbf{x}_0\mathbf{x}_2} + N_{\mathbf{x}_1\mathbf{x}_2} - N_{\mathbf{x}_0\mathbf{x}_1} - N_{\mathbf{x}_0\mathbf{x}_2}N_{\mathbf{x}_1\mathbf{x}_2}], \quad (1)$$

where $\bar{\alpha}_s = \alpha_s N_c/\pi$ is the strong coupling constant. Here, $N_{\mathbf{x}_0\mathbf{x}_1} \equiv N(\mathbf{x}_0, \mathbf{x}_1, Y)$ is the dipole-nucleus scattering amplitude, and $\mathbf{x}_0$ and $\mathbf{x}_1$ are two-dimensional vectors of the transverse position of the dipole ends. Alternatively, one can introduce the vector denoting the dipole size $\mathbf{r}_{01} = \mathbf{x}_0 - \mathbf{x}_1$, and the impact parameter $\mathbf{b}_{01} = (\mathbf{x}_0 + \mathbf{x}_1)/2$. Thus in general, the amplitude depends on the 4 degrees of freedom in transverse space and rapidity, $Y = \ln(1/x)$, playing the role of the evolution parameter. The transverse part of the LL kernel

$$\frac{dz}{z}\frac{d^2\mathbf{x}_2}{2\pi}\frac{x_{01}^2}{x_{02}^2 x_{12}^2}$$

is conformally (Möbius) invariant in 2 dimensions. Here, we introduced a more compact notation denoting $\mathbf{x}_{ij} \equiv \mathbf{x}_i - \mathbf{x}_j$, $x_{ij} = |\mathbf{x}_{ij}|$, and z is the longitudinal momentum fraction so that rapidity is $y = \ln 1/z$.

To obtain the solution of this equation, one has to specify an initial condition at $Y = Y_0$: $N^{(0)}_{\mathbf{x}_0\mathbf{x}_1} = N^{(0)}(\mathbf{x}_0, \mathbf{x}_1; Y = Y_0)$.

The amplitude $N_{\mathbf{x}_0\mathbf{x}_1}$ in (1) is given by the following correlator:

$$N_{\mathbf{x}_0\mathbf{x}_1} = \frac{1}{N_c}\,\mathrm{Tr}\langle 1 - U^\dagger(\mathbf{x}_0)U(\mathbf{x}_1)\rangle, \quad (2)$$

where the trace is done in the color space, and the eikonal factor U is defined as the path ordered exponential with the $SU(N)$ gauge fields (in the gauge $A_a^- = 0$):

$$U(\mathbf{x}) = P\exp\left\{i\int dx^- T^a A_a^+(x^-, \mathbf{x})\right\}. \quad (3)$$

The averaging $\langle \ldots \rangle$ in (2) is performed over an ensemble of classical gauge fields.

The next-to-leading logarithmic corrections to the BK equation have been computed in [50,52]. It would be instructive to perform the analysis of the BK equation

with the full next-to-leading logarithmic approximation. Because of the complicated form of this kernel we are not trying to solve it here. What we consider instead is the equation with two important modifications. The first one is the running coupling correction, which we analyze in Sec. VI of this paper. The second one is the subleading correction coming from the kinematical corrections, included in the form of the modified kernel proposed in [46].

The soft gluon approximation performed in [17] was crucial in order to factorize the branching kernel for the gluon emissions. In [46] a modified version of the kernel was proposed, which includes part of the subleading corrections coming from the kinematics. By taking into account an improvement in the kernel in which the value of the energy denominator is obtained from the invariant mass of the produced gluon pair, this leads to a new color dipole kernel which has the form

$$\frac{dz}{z} z \frac{d^2\mathbf{x}_2}{x_{01}^2}\left[K_1^2\left(\frac{x_{02}}{x_{01}}\sqrt{z}\right) + K_1^2\left(\frac{x_{12}}{x_{01}}\sqrt{z}\right) - 2K_1\left(\frac{x_{02}}{x_{01}}\sqrt{z}\right)K_1\left(\frac{x_{12}}{x_{01}}\sqrt{z}\right)\frac{\mathbf{x}_{02}\cdot\mathbf{x}_{12}}{x_{02}x_{12}}\right], \tag{4}$$

where K_1 is the modified Bessel function. The modified kernel becomes equivalent to the leading logarithmic kernel for $zx_{02}^2 \ll x_{01}^2$ and $zx_{21}^2 \ll x_{01}^2$ but differs significantly otherwise. To be precise, the production of larger dipole sizes is exponentially suppressed above the cutoff size which depends on the longitudinal momentum fraction of the soft gluon. The modified kernel introduces corrections at all orders beyond the leading logarithmic approximation. The suppression of the large dipole emission implies also a suppression of the diffusion in the impact parameter. An alert reader might notice that the above modified kernel is not conformally invariant. This is due to the fact that in [46] only part of the kinematical corrections were taken into account resulting in kernel (4). In general there should be also a cutoff on small dipoles, similarly to what was done in [53], which would yield conformally invariant kernel. We postpone the derivation and numerical analysis of such a kernel to a later work.

In what follows we will analyze both forms of the equations numerically, taking into account also running coupling corrections. We shall demonstrate that the sensitivity to the subleading corrections strongly depends on the type of approximation one is working on, i.e. whether the solutions are impact parameter dependent or not.

III. NUMERICAL METHODS

The BK equation was solved numerically by discretizing the scattering amplitude in terms of variables $(\log_{10} r, \log_{10} b, \cos\theta)$, where θ is the angle between impact parameter $\mathbf{b}$ and dipole size $\mathbf{r}$. We have assumed that the solution is rotationally invariant; this condition removes an additional angle from the equation which reflects the overall orientation of the dipole. To be precise, in the dipole-dipole scattering case this second angle reflects the orientation of one of the dipoles in two-dimensional transverse space. As we will see later, this simplifying assumption leads to slight violations of the conformal symmetry of the solution. The solution with full angular dependence will be discussed elsewhere. The amplitude $N(r, b, \cos\theta)$ was placed on a grid with dimensions $200_r \times 200_b \times 20_\theta$. It was found that the number of points in the grid was less important than the absolute limits on the grid and the number of integration regions. The limits of the grid were $10^{-8} \rightarrow 10^8$ in r and b. We note that the grid limits of r and b cannot not be set independently due to the correlations in dipole size and impact parameter. The initial condition $N^{(0)}$ at rapidity $Y = 0$ was chosen as in Ref. [44] to be of the Glauber-Mueller [54,55] form

$$N^{(0)} = 1 - e^{-10r^2 e^{-(b^2/2)}}. \tag{5}$$

This is the form of the scattering amplitude at the initial rapidity. We note that in this analysis the constants are arbitrary and have not been fit to any experimental data. The initial condition (5) has the property that it reaches unity when the dipole size is large and it goes to zero for large values of the impact parameter by the steeply falling profile in b. The amplitude is evolved in small steps $\Delta Y = 0.2$ as it was found that the smaller spacings had no significant effect on the accuracy of the evolution of the amplitude. Below, we denote integration over $\mathbf{x}_2$ simply by $\int_{\mathbf{x}_2}$ and this is understood to absorb the kernel as well as a measure $d^2\mathbf{x}_2$ for ease of notation in this section. The basis of the method for the solution is the same as utilized in Ref. [44] and we briefly outline it below. After one step of evolution from Y_0 to $Y = Y_0 + \Delta Y$ Eq. (1) becomes

$$N_{x_0x_1}(Y_0 + \Delta Y) = N_{x_0x_1}(Y_0) + \int_{\mathbf{x}_2}\int_{Y_0}^{Y_0+\Delta Y}[N_{x_0x_2} + N_{x_1x_2} - N_{x_0x_1} - N_{x_0x_2}N_{x_1x_2}]. \tag{6}$$

The lowest approximation for this equation is

$$N^{(1)}_{x_0x_1} = N^{(0)}_{x_0x_1} + \Delta Y \int_{\mathbf{x}_2}[N^{(0)}_{x_0x_2} + N^{(0)}_{x_1x_2} - N^{(0)}_{x_0x_1} - N^{(0)}_{x_0x_2}N^{(0)}_{x_1x_2}]. \tag{7}$$

The superscript 1 denotes the first approximation while the superscript 0 denotes the initial condition. The accuracy of the equation is measured by the relative difference of the approximation defined by $|(N^{(1)}_{x_ix_j} - N^{(0)}_{x_ix_j})/N^{(0)}_{x_ix_j}|$. If this is less than some required accuracy, then the value of $N^{(1)}_{x_ix_j}$ is taken as the scattering amplitude at $Y = Y_0 + \Delta Y$. In our case the relative accuracy was set to equal 0.02. If the accuracy condition is not satisfied, then we can find a second approximation by utilizing linear interpolation $N^{(2)}_{x_ix_j} = \frac{Y(N^{(1)}_{x_ix_j} - N^{(0)}_{x_ix_j})}{\Delta Y} + N^{(0)}_{x_ix_j}$. By using this linear

interpolation in the right-hand side of (6) the expression for the next iteration can be attained:

$$N^{(2)}_{x_0x_1} = N^{(0)}_{x_0x_1} + \frac{\Delta Y}{2}\int_{\mathbf{x}_2}[N^{(0)}_{x_0x_2} + N^{(0)}_{x_1x_2} - N^{(0)}_{x_0x_1} - N^{(0)}_{x_0x_2}N^{(0)}_{x_1x_2}] + \frac{\Delta Y}{2}\int_{\mathbf{x}_2}[N^{(1)}_{x_0x_2} + N^{(1)}_{x_1x_2} - N^{(1)}_{x_0x_1} - N^{(1)}_{x_0x_2}N^{(1)}_{x_1x_2}] + \frac{\Delta Y}{6}\int_{\mathbf{x}_2}[N^{(1)}_{x_0x_2} - N^{(0)}_{x_0x_2}][N^{(1)}_{x_1x_2} - N^{(0)}_{x_1x_2}]. \quad (8)$$

If the accuracy condition mentioned earlier is still not satisfied, this can be repeated by utilizing $N^{(n)} = \frac{Y(N^{(n-1)} - N^{(0)})}{\Delta Y} + N^{(0)}$. The number of iterations required to reach this level of accuracy varies on how close one is to the initial condition and the exact form of the equation (kernel used, running coupling form, etc.). Near the initial conditions it could take upwards of ten iterations, but far away from the initial condition two or three iterations are usually sufficient to obtain the accuracy assumed. With this in mind an algorithm was written so that the iteration number was not fixed but only continued until the desired accuracy was reached. Once the amplitude has been found for $Y = Y_0 + \Delta Y$, that takes the place of $N^{(0)}$ in the numerics and the procedure is repeated to find the amplitude at $Y = Y_0 + 2\Delta Y$. In this way the amplitude is evolved numerically to higher rapidities.

As was mentioned earlier the number of points in the grid was not as important as the number of integration regions the program executes to get a good solution. For our limits it was found that breaking the range into at least 20 integrations was needed. This meant there would be an incredible number of function evaluations and in order to reach any useful rapidity on a standard dual-core machine would take upwards of a month. The program was parallelized using the Message Passing Interface library so it could be used with computer clusters to run the program. Each run took approximately three days to run on 32 linked 3 GHz processors and generated a total of 5 gigabytes of data.

IV. RESULTS WITHOUT IMPACT PARAMETER DEPENDENCE

In this section we briefly present the results of the numerical solution without impact parameter dependence. This was of course done in many previous works [33–35,56], but we repeat this analysis below for several reasons. First of all, we wanted to have a benchmark for the comparison of the solutions. Second, we wanted to perform the analysis of the modified BK equation with the Bessel function kernel, a computation not performed earlier in the literature.

The BK equation can be evaluated without the impact parameter or angular dependence, and this greatly reduces the time needed to evolve the scattering amplitude. The initial condition used in this case is taken to be

$$N^{(0)} = 1 - e^{-r^2}, \quad (9)$$

without an impact parameter profile. This form goes to unity as the dipole size gets large and has a narrow transition region from 0 to 1. The absolute limits on the dipole size here are $10^{-10} \rightarrow 10^{10}$ and the number of points in the grid is 5000. These results are for fixed coupling $\bar{\alpha}_s = 0.1$; the case with running coupling is considered in Sec. VI.

The solid lines shown in the left graph in Fig. 1 correspond to a set of scattering amplitudes found from the LO BK equation at constant rapidity. The result has the well known form of a traveling wave with rapidity playing the role of the time in the evolution. As rapidity increases the front moves towards the small values of dipoles.

Next, we performed the evolution of the modified equation with the Bessel function kernel, and the solutions are illustrated by the dashed lines in Fig. 1. The normalization of the amplitude in the dilute regime is much smaller than the LO case. This is to be expected as the K_1 functions fall off faster than the powerlike LO kernel. The speed of this evolution can be quantified by the evaluation of the saturation scale. The equation to define the saturation scale is

$$\langle N(r = 1/Q_s, Y)\rangle = \kappa, \quad (10)$$

where κ is a constant between 0 and 1. It determines the point at which nonlinearities begin to become important in the evolution equation. In all the analysis in this paper $\kappa = 0.5$ was chosen. Based on the results of [40,57] we expect the saturation scale to have the following form:

$$Q_s^2(Y) = Q_0^2 \exp\left[\bar{\alpha}_s\left(\frac{\chi(\gamma_c)}{1-\gamma_c}Y - \frac{3}{2(1-\gamma_c)}\ln Y\right)\right], \quad (11)$$

where $\chi(\gamma)$ is the BFKL kernel eigenvalue and $\gamma_c = 0.62$. This gives $\frac{\chi(\gamma_c)}{1-\gamma_c} = 4.88$ and $\frac{3}{2(1-\gamma_c)} = 2.39$ for the LO kernel. The second term in the exponent is a correction of less than 10% compared to the first term for the rapidities which we are considering so we take the saturation scale to be parameterized in this paper by

$$Q_s^2 = Q_0^2 e^{\lambda_s \bar{\alpha}_s Y}, \quad (12)$$

where λ_s is extracted from the numerical solution and Q_0 is a normalization term. The extracted value for the saturation exponent is $\lambda_s = 4.4$ for both the LO and Bessel function kernels. The exponent was extracted for both $\bar{\alpha}_s = 0.1$ and $\bar{\alpha}_s = 0.2$ and it was found to be the same. The values of λ_s are evaluated in the region of rapidities where the exponent is constant, i.e. nearly asymptotic. We observed that for the lower rapidities near the initial condition the exponent slowly increases and at very large rapidities the exponent begins to decrease. The latter effect is due to the absolute limits of the dipole size (or the box in which the equation is being solved). This strongly affects the solution, and one of the effects is to slow down the evolution. This effect can be clearly seen in Fig. 1, where the three regimes are distinct. The first regime is where there are a lot of preasymptotic

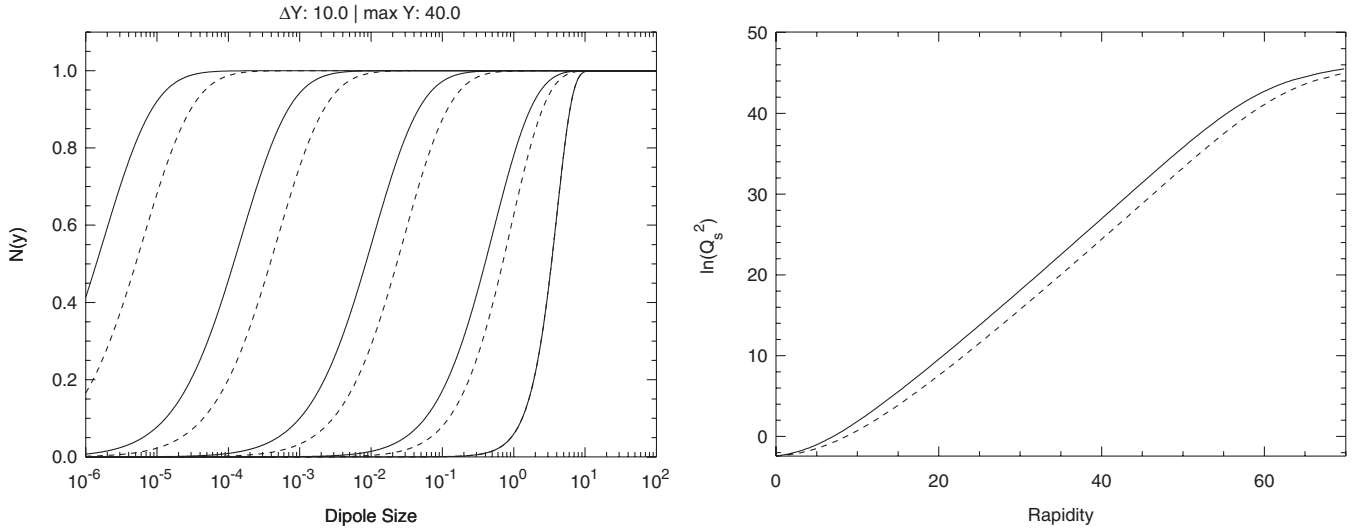

FIG. 1. Left: Comparison between the LO kernel (solid lines) and the kernel with Bessel functions, (4) (dashed lines), at constant rapidities. The solid line at the far right is the initial condition for both cases, and each line to the left represents an evolution in ten units of rapidity to a maximum of $Y = 40$. Right: Plot of the logarithm of the saturation scale as a function of rapidity. The solid line represents the evaluation with the LO kernel, and the dashed line represents the solution with the Bessel kernel. The slope of the curve gives λ_s, and the three regimes of evolution can be seen. This calculation was done for the fixed coupling case and without the impact parameter.

effects, there is strong dependence on the initial condition, and the speed of evolution increases (approximately between 0 and 34 units of rapidity), the regime where evolution is a constant (approximately between 34 and 47 units of rapidity), and finally the regime where box size limits growth (rapidity 47+). These values clearly shift with box size and they also change depending on the value of $\bar{\alpha}_s$ and to a lesser extent which kernel is used.

The extracted value of the exponent of the saturation scale is consistent with the theoretical predictions of [40,57]. What is, however, surprising at first is the fact that the asymptotic value of λ_s is nearly the same for the modified version of the equation. This is also evident by investigating the right plot in Fig. 1, where the two saturation scales grow with rapidity in almost exactly the same way. This effect can be easily understood by inspecting the form of the modified kernel:

$$Q_{01}^2\Big[K_1^2(Q_{01}x_{02}) + K_1^2(Q_{01}x_{12}) - 2K_1(Q_{01}x_{02})K_1(Q_{01}x_{12}) \times \frac{x_{02}\cdot x_{12}}{|x_{02}||x_{12}|}\Big]. \tag{13}$$

Here $Q_{01} = \sqrt{z}/x_{01}$ and $z = e^{-y}$. When Q_{01} is small and the arguments of the Bessel functions are small, this expression reduces to the LO kernel. At large rapidities where the exponent λ_s is evaluated, z is small and thus Q_{01} is also small. The difference between the modified kernel and the LO kernel comes from the regime where the dipole sizes x_{12} and x_{02} are large, that is, when

$$x_{12}, x_{02} \gg \frac{1}{Q_{01}}.$$

In this large dipole regime (and for large rapidities), the scattering amplitude is close to unity, and the right-hand side of the BK equation goes to zero so there is no contribution from that regime. This means that the effect of the infrared modification of the kernel of the type (13) is negligible when the nonlinear evolution is considered. The modified kernel (13) was shown to reproduce the double-logarithmic terms in the exact next-to-leading logarithmic calculation. These types of terms are known to come from the scale choice in the amplitude [58–61].

Two comments are in order here. The first observation is that, as we shall see later, the presence of the impact parameter changes the dynamics significantly, and in this case the dependence on the form of the kernel is more pronounced. In particular, in this case we do find the differences in the evolution speed due to the cutoffs in the infrared. The second comment is that, in order to address the question of the scale choices, one needs to take into account the corrections beyond the BK equation. The BK equation is highly asymmetric with respect to the target and projectile and therefore cannot address the problems of all the scale choices. The corrections would necessarily have to include the Pomeron loops in order to make the evolution symmetric with respect to the target and projectile. Such a formulation has been implemented in a Monte Carlo approach [51,53,62,63] with Pomeron loops effectively taken via so-called dipole swing and with cutoffs in both the infrared and ultraviolet regions.

V. RESULTS WITH IMPACT PARAMETER DEPENDENCE

A. Dependence on the dipole size

In this section we discuss the results which include the impact parameter dependence as well as the angular dependence between the dipole sizes and the impact parameter orientation. Let us first investigate the dependence of the scattering amplitude on the dipole size with the fixed impact parameter value. Figure 2 shows the case of the LO simulation with $\bar{\alpha}_s = 0.1$. The scattering amplitude at small dipole sizes evolves in a similar manner as in the case without the impact parameter.

At large dipole sizes the situation is drastically changed with respect to the translationally invariant case. Here, we observe that the amplitude drops down from the initial distribution and forms a second evolution front. This drop is very rapid compared to the expansion evolution of the small dipole size regime or the large dipole size regime at higher rapidities. The evolution of the front at large dipole sizes can be best seen in Fig. 2(b), where the steps in rapidity are greater. As discussed in [44] there is a clear physical reason for this effect. For a large dipole, its end points are in the region where there is no gauge field. In this situation the gauge field correlator

$$N(\mathbf{x}, \mathbf{y}) = \frac{1}{N_c} \mathrm{Tr}\langle 1 - U^\dagger(\mathbf{x}) U(\mathbf{y})\rangle \tag{14}$$

vanishes because $U(\mathbf{x}) \simeq U(\mathbf{y}) \simeq 1$. In this case the dipole is larger than any of the other scales in the problem, including the impact parameter of the collision. In other words, this situation corresponds to the setup of very large dipole scattering on a localized target, and in this case the dipole misses the target, resulting in the vanishing scattering amplitude. This effect is not present in the case where impact parameter dependence is neglected simply because this approximate case corresponds to the infinitely large target.

The fact that the amplitude drops for large dipole sizes is inherently related to the finite extension of the interaction region. This effect is thus tied to the impact parameter dependence of the scattering amplitude (see, for example, Fig. 7 in [44] and discussion thereabout). In the perturbative evolution the large dipole sizes are still accessible at sufficiently large rapidities and hence lead to the generation of the power tails in impact parameter space. In the realistic case of confining QCD, one would expect the large dipole sizes to be cut off by the confinement scale. The amplitude for large dipole sizes would therefore be set to zero, and it is expected that the resulting impact parameter expansion will be significantly slowed down and the functional dependence on the rapidity changed from powerlike to exponential (or Gaussian depending on the details of the cutoff). The simulation of the case with the massive kernel is currently under investigation.

It is interesting to investigate the dipole size dependence of the amplitude at large values of the impact parameter as in Fig. 3. There the initial condition sets the amplitude to zero. The evolution quickly changes this value, and a unique feature of the solution develops. Namely, a peak is formed with the center at the dipole size value which is exactly twice the impact parameter value. The peak grows until saturation is reached and the evolution of the fronts proceeds to the infrared and ultraviolet regions. The discussion about the origin of peaks is given in Sec. V D.

We have repeated this analysis for the case of the modified kernel. As can be seen in Fig. 4(a) the evolution in the

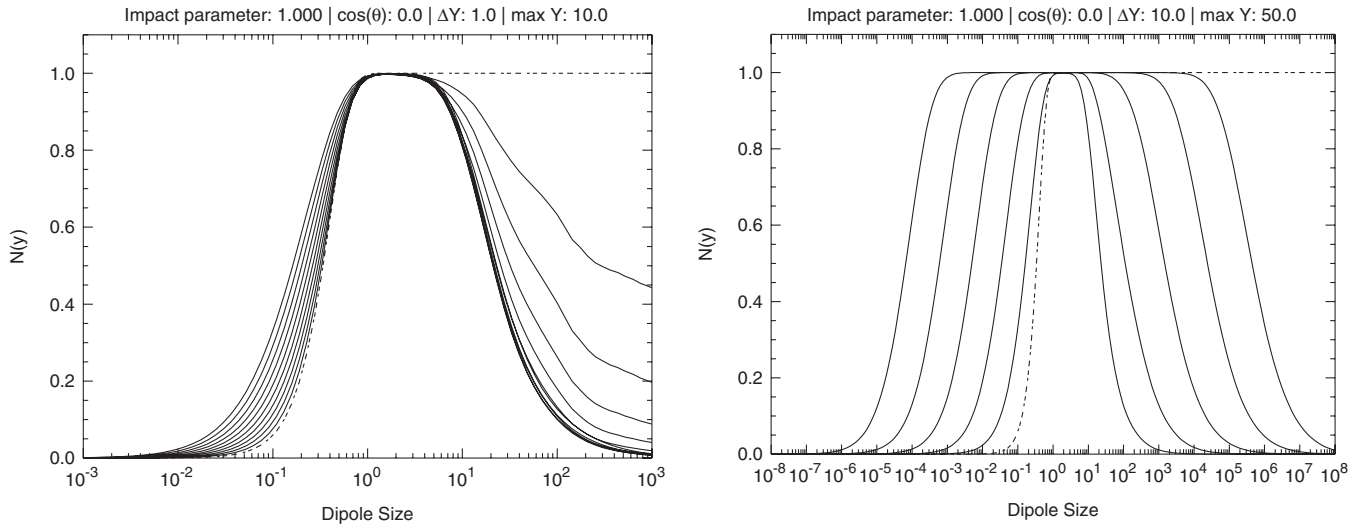

FIG. 2. Graphs of the scattering amplitude $N(x, b, \theta, Y)$ at various constant rapidities for the calculation with impact parameter dependence. Left: The individual lines correspond to the rapidity intervals $\Delta Y = 1.0$ up to rapidity of $Y = 10$. Right: The individual lines correspond to the rapidity intervals of $\Delta Y = 10$ and the maximal rapidity is $Y = 50$. The dotted line represents the initial condition which is the same in both graphs. The impact parameter and angle are fixed for both graphs at $b = 1.0$ and $\cos(\theta) = 0$.

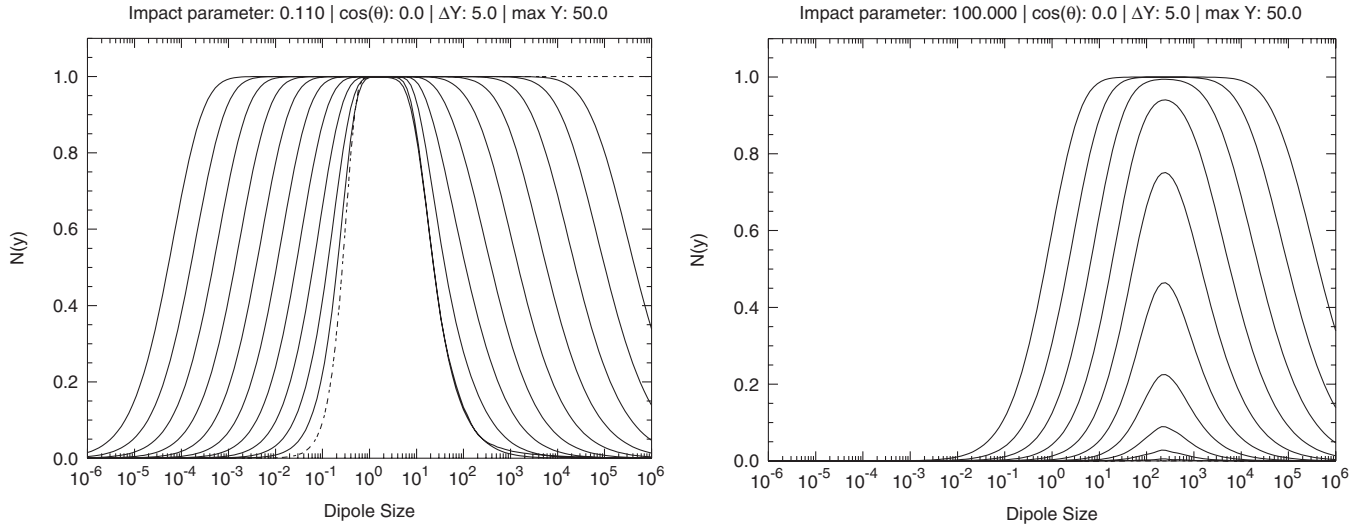

(a) $b = 0.11$ (b) $b = 100$

FIG. 3. Graphs of the scattering amplitude at different constant rapidities for two different impact parameter values. The dotted line represents the initial condition which is the same in both graphs; however. the initial condition is near zero on the second graph with $\cos(\theta) = 0$. Each line past the initial condition represents five rapidity units to a maximum of 50.

small dipole regime is now quite different from the LO kernel. The evolution is significantly slower in this regime for the Bessel function kernel. Interestingly, the evolution in the large dipole region is slowed too but not as much as for small dipoles. This is best illustrated in Fig. 4(b), where the evolution has been performed to large rapidities. The larger influence of the cutoff from the Bessel function in the impact parameter case is the result of the fact that it is sensitive to the region of large dipole sizes where the amplitude is not saturated. On the other hand, in the local case the infrared region is completely cut off by the saturation scale, and therefore any cutoffs in this regime do not change significantly the speed of the evolution although they have significant impact on the normalization of the saturation scale. One has to note that in the linear case such cuts are important both in the forward and in the non-forward cases. However, the forward (which is equivalent to the local case) linear BFKL evolution is well defined due to the conservation of the number of gluons in the t channel, when viewed in the momentum space. On the

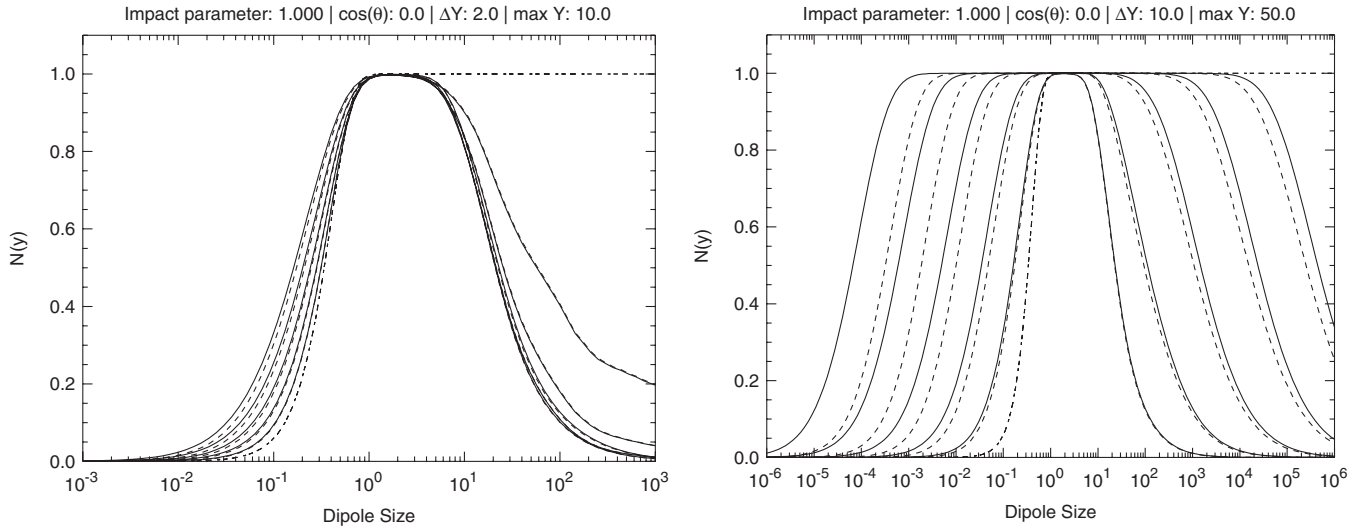

FIG. 4. Graphs of the scattering amplitude as a function of the dipole size at various constant rapidities for fixed impact parameter $b = 1.0$ and angle $\cos(\theta) = 0$. The solid lines are for the LO kernel, and the dashed lines correspond to the Bessel kernel. The initial distribution is equivalent for both kernels and is represented by the dotted-dashed line. On the left graph each line represents a change in two units of rapidity to a maximum of ten, and on the right graph each line represents a change in ten units of rapidity to a maximum of 50.

other hand, in the nonlinear case the triple Pomeron vertex allows for a changing number of gluons in the t channel and therefore the evolution necessarily involves off-forward gluon Green's functions. In this sense, the local case in the nonlinear evolution is an approximation, and therefore in general one cannot expect that the next-to-leading corrections will have the same impact. An example is the situation when the strong coupling is running, as the impact parameter dependent solution to BK is sensitive to the details of the regularization of the running coupling whereas the local nonlinear evolution is generally insensitive. We note, however, that in order to firmly establish the role of the next-to-leading-order corrections of the BK one needs to solve the exact equation at this order.

B. Impact parameter profile of the scattering amplitude

Dependence of the dipole amplitude on the impact parameter is illustrated in Fig. 5. The leftmost dashed-dotted line is the initial condition Eq. (5), which has a very steep profile in the impact parameter. The evolution of the scattering amplitude towards large values of the impact parameter follows the diffusion of large dipoles. The speed of this evolution can be extracted numerically and is determined by the expansion of the black disk radius. We will discuss this quantity in detail in the next section.

Evolution in the impact parameter shows a marked change in profile from the steeply falling exponential in the initial condition. This is better illustrated in the right plot in Fig. 5, where we replot the impact parameter using the logarithmic scale in the scattering amplitude. The profile changes from the exponential to a power tail at small scattering amplitudes. This can be seen as an ''ankle'' in the curves of constant rapidity. The origin of this powerlike tail was discussed in detail in Ref. [44]. These power tails are also present in the modified kernel. In the latter case, however, there is a slower evolution of the profile towards the large values of impact parameters. There also exists a nontrivial angular dependence which is most prominent in the cases of large dipole size or impact parameter but for very specific configurations. In the case when the dipole size is much smaller or much larger than the impact parameter, the solution does not depend much on the spatial orientation of the dipoles. On the other hand, for the case when the dipole size is twice as large as the impact parameter, there exists strong angular dependence. This angle θ is defined as the angle between the dipole and the impact parameter, as illustrated in Fig. 6. The effects of this angle are best illustrated in Figs. 7(a), 7(b), 8(a), and 8(b). In these figures the scattering amplitude is plotted as a function of both dipole size and impact parameter for different choices of the angle θ. The amplitude has a peak when at $r = 2b$ for both orientations as is shown in both plots in Fig. 7. Note, however, that the peak is distinctively sharper for the ''aligned'' dipole configurations, when $\cos\theta = 1.0$ or -1.0, than for the ''perpendicular'' configuration. This is also illustrated in Fig. 9, where the dependence on the angle is shown. For values that are near the $r = 2b$ point there are enhancements at $\cos\theta = 1.0, -1.0$ and this is present in both kernels. These effects can be seen in both plots in terms of dipole size and impact parameter. It is interesting to note that the peak is present in the case of scattering amplitude versus dipole size even when $\cos\theta = 0.0$. On the other hand, such structure is absent for this configuration in the impact parameter profile with a fixed dipole size. It is also evident in Fig. 8 that the amplitude is flat in the impact

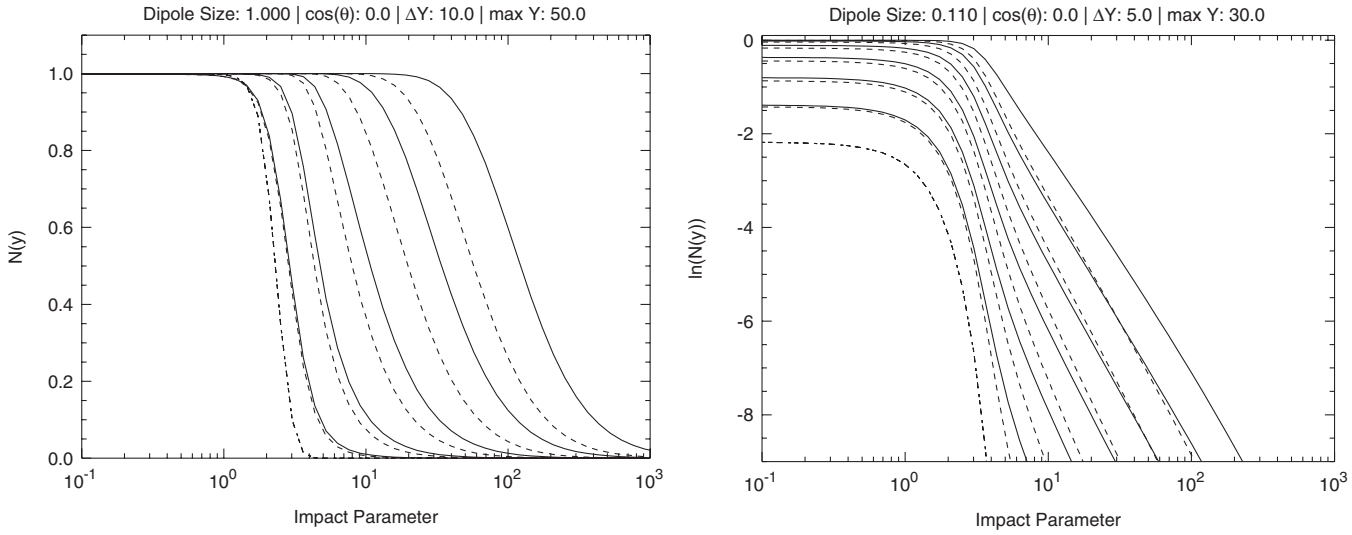

FIG. 5. Graph of the scattering amplitude as a function of the impact parameter for fixed dipole size $r = 1.0$. The solution with the case of the LO kernel is plotted as a solid line and with the modified kernel (13) as a dotted line. The dotted-dashed line on the left is the initial condition. Each line thereafter represents an increase in rapidity of ten units to a maximum of 50. Right plot: The same but for the dipole size $r = 0.11$ and in logarithmic scale for the amplitude.

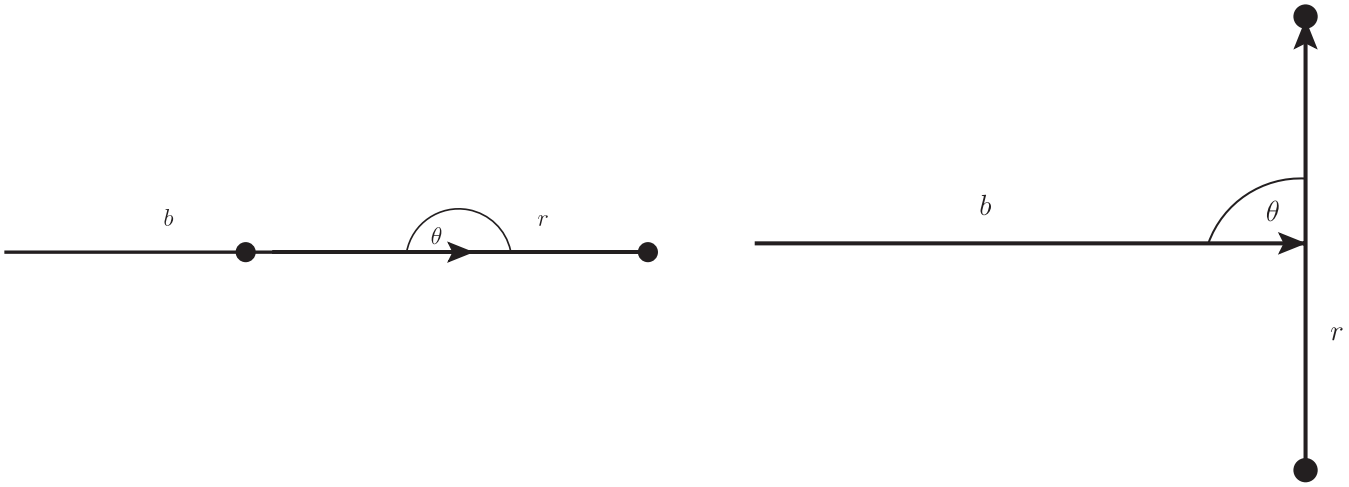

FIG. 6. Two configurations, aligned and perpendicular, of the dipole orientation with respect to the impact parameter.

parameter when the dipole size is much larger than b. We will demonstrate that all these effects can be easily understood from a conformal representation of the amplitude in Sec. V D.

C. Saturation scales

The saturation scale in the impact parameter dependent scenario is again defined by the following equation:

$$\langle N(r = 1/Q_s, b, \theta, Y)\rangle = \kappa, \tag{15}$$

where κ is a constant. In all the following analysis we have set $\kappa = 0.5$. It is important to note that in this case the form of the amplitude admits two solutions to the above equation. As is evident from Fig. 2 one solution for the saturation scale is for a larger dipole size and one for a smaller dipole size. The saturation scale Q_s always refers to the solution where the dipole size is smaller. We have found that the slope in rapidity of the saturation scale Q_s increases for low values of rapidities and then reaches an approximately constant value, and for ultrahigh rapidities it starts to decrease. The first effect is caused by the preasymptotic contributions; the latter effect is caused by the finite size of the grid. We have found that the effects of the grid can be neglected below the rapidities of order ~60. The saturation scale as a function of the rapidity is shown in the left plot in Fig. 10. The solid line shows the calculation in the case of the LO kernel and the dashed line is for the Bessel kernel. It is clear that the dependence on the rapidity is exponential as expected for the computation with a fixed value of the coupling. The numerical value

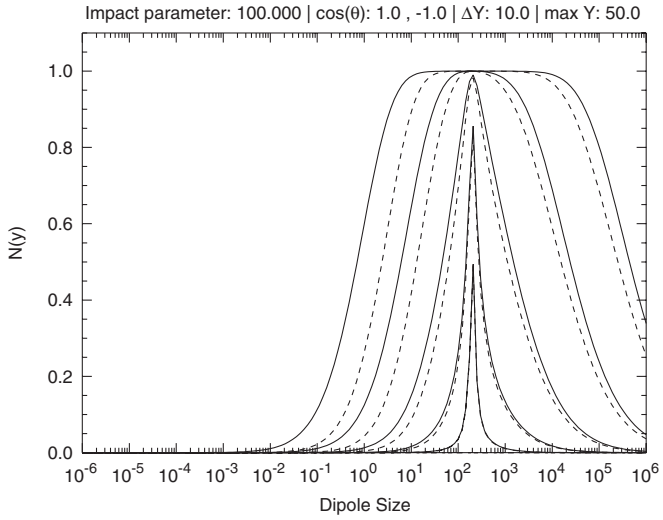

(a) $\cos(\theta) = 1.0, -1.0$

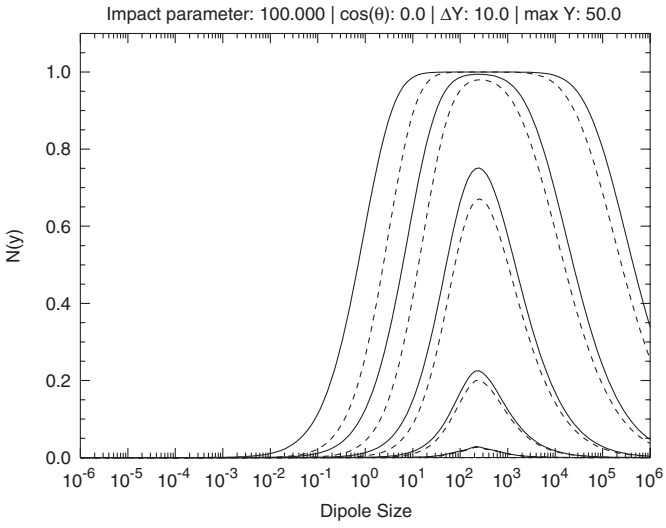

(b) $\cos(\theta) = 0.0$

FIG. 7. Graphs of the scattering amplitude versus the dipole size for fixed impact parameter $b = 100.0$ and various rapidities and angles. The initial condition is the same in all graphs and it is near zero; each curve represents an increase in ten units of rapidity to a maximum of 50. The LO kernel (solid lines) and the Bessel kernel (dotted lines) are plotted on the same graph.

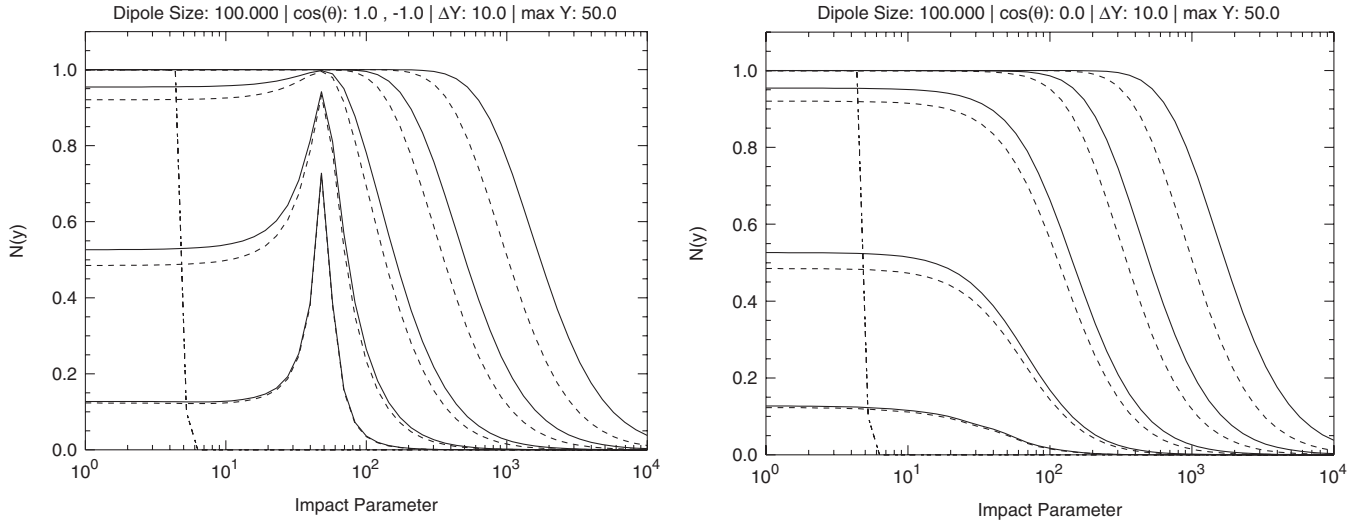

(a)$cos(\theta) = 1.0, -1.0$ (b)$cos(\theta) = 0.0$

FIG. 8. Graphs of the scattering amplitude versus the dipole impact parameter for constant dipole size $r = 100.0$ and various rapidities. The initial condition is the same in all graphs and it is the steeply falling dotted-dashed curve, which is the same for both the evolution with the LO kernel (solid lines) and the Bessel kernel (dotted lines). Each curve represents an increase in ten units of rapidity to a maximum of 50.

of the exponent governing the rapidity dependence of the saturation scale extracted in the LO kernel case is $\lambda_s = 4.4$; see (16). The value of the exponent extracted for the evolution with the Bessel kernel was found to be $\lambda_s = 3.6$. Clearly, the subleading effects of the modified kernel cannot be neglected here, which has to be contrasted with the case without the impact parameter.

In the case when the impact parameter is much larger than the inverse of the saturation scale the exponent in rapidity is independent of the impact parameter value. This means that the saturation scale has a factorized form:

$$Q_s^2(Y, b) = Q_0^2 \exp(\bar{\alpha}_s \lambda_s Y) S(b). \tag{16}$$

This is demonstrated in Fig. 10, where the small dipole saturation scale is shown as a function of the impact parameter for two different values of rapidity. The power tail $1/b^4$ is clearly prominent. There is a significant

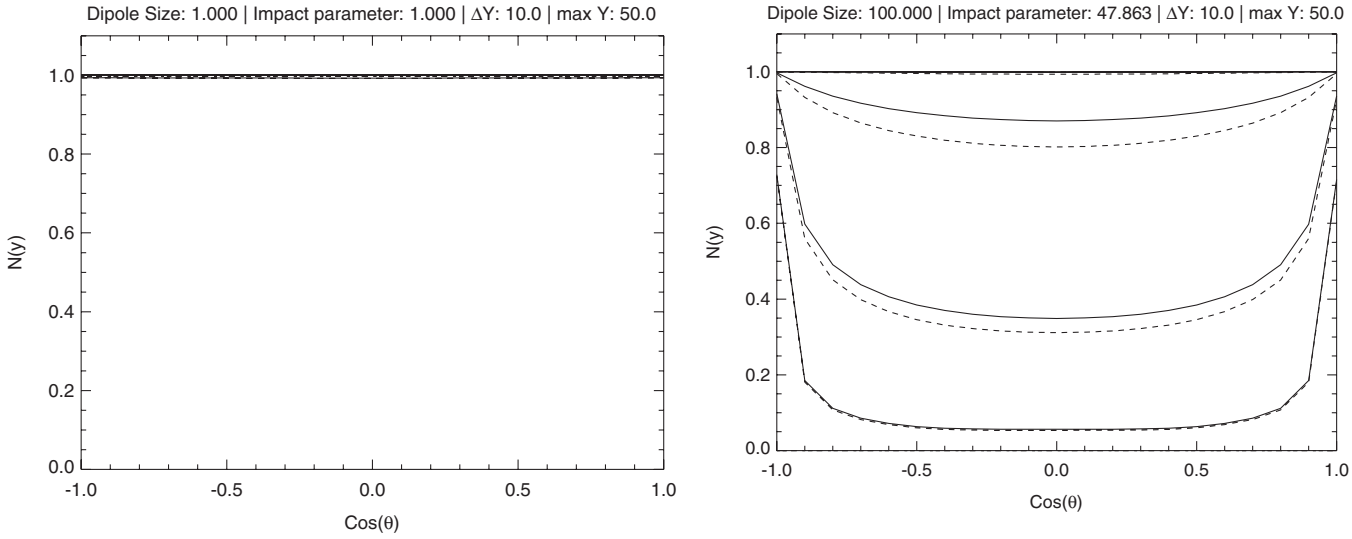

(a)$r = 1.0$ $b = 1.0$ (b)$r = 100.0$ $b = 47.8$

FIG. 9. Graphs of the scattering amplitude versus the angle. Both have the LO kernel (solid line) and the Bessel kernel (dashed line) graphed on them. The first graph shows no angular dependence, and the second shows a marked increase at values of $\cos(\theta) = 1.0, -1.0$ which accounts for the difference in peaks in Figs. 7 and 8.

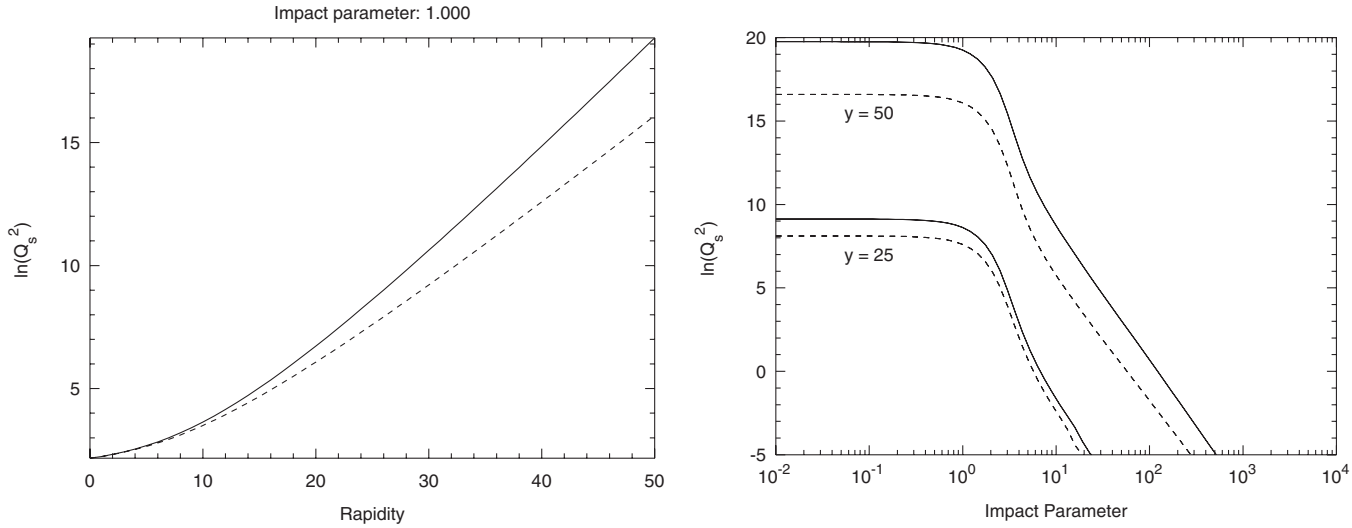

FIG. 10. Left: Plot of the saturation scale as a function of rapidity. The solid line corresponds to the LO simulation, and the dashed line is the saturation scale of the Bessel kernel. The impact parameter is fixed at $b = 1.0$. Right: The dependence of the saturation scale on the impact parameter for two different values of rapidity. Solid line: the LO kernel; dashed line: the Bessel kernel. Strong coupling is fixed at $\bar{\alpha}_s = 0.1$.

difference between the saturation scale from the Bessel function kernel and the LO kernel.

The second solution of Eq. (15), which shall be called $Q_{sL}(Y, b)$, gives the saturation scale at a large dipole size. As mentioned before, the fact that the amplitude expands very fast towards large dipole sizes is due to the fact that the calculation is based on the lowest order of the perturbation theory. In reality, the behavior of the amplitude in this region when $r \sim 1/\Lambda_{\mathrm{QCD}}$ is going to be heavily modified by the nonperturbative effects of confinement. Therefore one has to regard the large Q_{sL} as more of an academic interest rather than the quantity of physical meaning.

Nevertheless, the same analysis that was performed on Q_s can be performed on Q_{sL} with the parameterization of this saturation scale taken to be

$$Q_{sL}^2 = Q_{0L}^2 e^{-\lambda_{sL}\bar{\alpha}_s Y}, \tag{17}$$

where once again Q_{0L} is a normalization term and the minus sign in the exponent is because the evolution is now moving towards larger dipole sizes.

The extracted value for the LO kernel is $\lambda_{sL} = 6.0$ and for the Bessel function kernel $\lambda_{sL} = 5.6$. The difference between these two exponents is now about 7%, and it can be seen in Fig. 11 that these curves are much closer than in Fig. 10.

The reason for these effects can be understood by again inspecting the form of the Bessel kernel

$$Q_{01}^2\Big[K_1^2(Q_{01}x_{02}) + K_1^2(Q_{01}x_{12}) - 2K_1(Q_{01}x_{02})K_1(Q_{01}x_{12}) \times \frac{x_{02}\cdot x_{12}}{|x_{02}||x_{12}|}\Big]. \tag{18}$$

When x_{01} is small then Q_{01} is large and the cutoff is on dipoles such that $x_{02} > 1/Q_{01}$ is very large. This means that unless x_{02} is very large (which would also correspond to large x_{12}) then the modified kernel is very close the LO kernel. It is this limitation of the phase space of the modified kernel that causes the dipole saturation scale for large dipoles to have a rather modest difference between the Bessel and LO cases. At this point it is worth noting that the Bessel kernel does not exhaust all the kinematical effects. To be more precise, we would expect that the kinematical cuts are resulting in the kernel which is also conformally invariant. This will give cuts on both small and large dipole sizes and further reduce the evolution speed.

One can also define from (15) a scale which corresponds to the extension in impact parameter space. This scale is the radius of the black disk. This can be done by solving this equation for b rather than for the dipole size.

We therefore define the black disk radius in impact parameter B_s by solving the equation

$$\langle N(r, b = B_s, \theta)\rangle = \kappa, \tag{19}$$

with respect to b and where once again $\kappa = 0.5$ is chosen. We assume the exponential form for the behavior of the impact parameter radius as a function of rapidity:

$$B_s^2 = B_{s0}^2 e^{\lambda_{Bs}\bar{\alpha}_s Y}. \tag{20}$$

Here B_{s0} is a normalization term and λ_{Bs} is extracted from the numerical solution. We have found for the LO kernel $\lambda_{Bs} = 2.6$ and for the modified kernel $\lambda_{Bs} = 2.2$. This is approximately half of the λ_s in the case of the LO kernel. As argued before [44,64] this is due to the fact that the amplitude depends on one variable, which in the case of

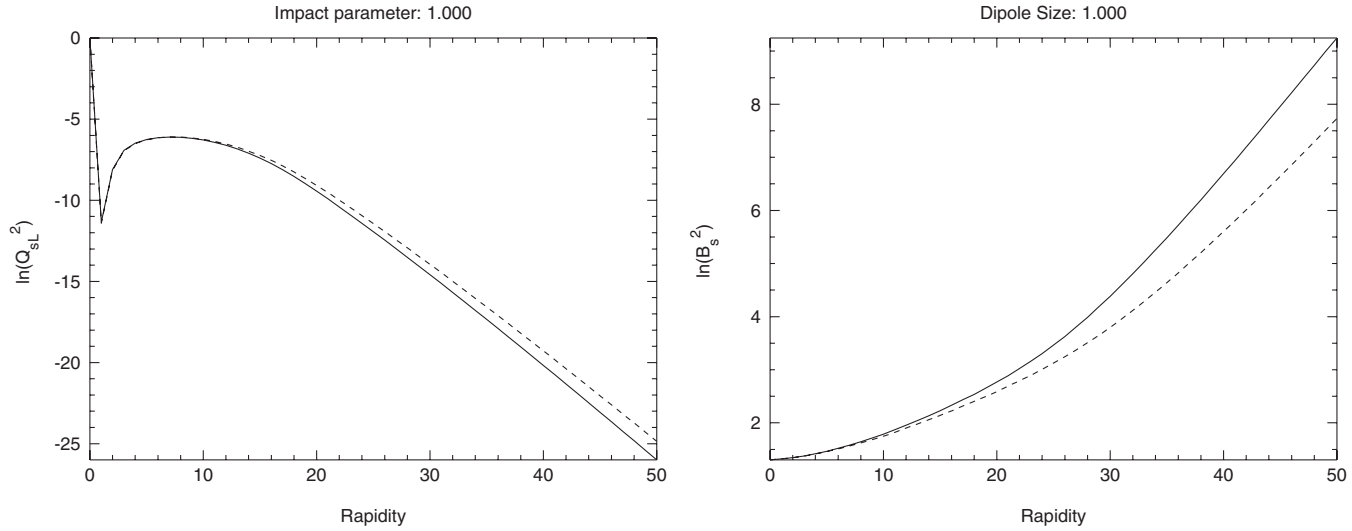

FIG. 11. Left: Plot of the saturation scale for a large dipole size as a function of rapidity. The solid line represents the result using the LO kernel, and the dashed line represents the result using the Bessel kernel. The impact parameter is fixed at $b = 1.0$. Right: Plot of the black disk radius defined by Eq. (19) for the LO kernel (solid line) and the modified kernel (dashed line). The dipole size is fixed at $r = 1.0$.

the configuration $b \gg r$ is proportional to r/b^2. This immediately means that the impact parameter dependence in rapidity is twice slower than the one of the dipole size. The computation for the Bessel function kernel shows that it does not hold as closely in this case because in such a case we do not have an exact conformal symmetry. These properties will be explained in more detail in the next section.

The simulations with different values of the fixed coupling were also performed. The results are summarized in Table I. It can be seen that the exponents for the LO kernel do not depend on the value of the coupling, which is the expected behavior as this is a fixed order calculation. On the other hand, the exponents extracted for the modified kernel significantly differ, exhibiting the nonlinearity in the coupling constant. The exponents are further reduced with respect to the LO values which is due to the resummation of the subleading terms in $\ln 1/x$.

The dependence on the initial conditions was also tested. As an alternative, we have taken the second initial condition to be modified by the cutoff in the large dipole size

$$N^{(0)}_{(2)} = N^{(0)} \exp(-r\mu), \tag{21}$$

where $\mu = 1/5$. The exponents are also shown in Table I [LO (2)]. We observe a modest variation of the exponents with the change on the initial condition. The most significant change is for the large dipole saturation scale. This is to be expected as in this region the two initial conditions differ significantly.

In Fig. 12(a) the amplitude as a function of the dipole size and various impact parameters is shown. It is interesting that for large dipole sizes the amplitude has the same front for all the impact parameters. This is related to the properties of the solutions stemming from the conformal symmetry; see Sec. V D. In Fig. 12(b) we show the saturation region for the solution with the impact parameter. Unlike in the local case (without the impact parameter) here the saturation region has a "V" shape in $(Y, \ln r)$ space, which is moving towards higher rapidities and larger dipole sizes as the impact parameter increases. Different shaded areas correspond to three different impact parameters. Again, the common front for the different values of b is clear. The distortion at lower rapidities and for a small impact parameter stems from the initial conditions.

TABLE I. Summary of extracted saturation exponents for solutions with the impact parameter. (1) means Glauber-Mueller initial conditions, and (2) means Glauber -Mueller with the exponential cutoff on the large dipole sizes.

	λ_s	λ_{sL}	λ_{sB}
LO kernel (1) $\bar{\alpha}_s = 0.1$	4.4	6.0	2.6
LO kernel (2) $\bar{\alpha}_s = 0.1$	4.4	5.8	2.6
Modified kernel $\bar{\alpha}_s = 0.1$	3.6	5.8	2.2
LO kernel $\bar{\alpha}_s = 0.2$	4.4	5.9	2.6
Modified kernel $\bar{\alpha}_s = 0.2$	2.5	5.2	2.0

D. Conformal representation and properties of the amplitude

Most of the features observed in the numerical solutions can be explained by using the conformal representation of the solution for the scattering amplitude. In general the representation can be shown to be of the form [4]

$$F(\mathbf{r}_0, \mathbf{r}, \mathbf{b}; Y) = \int_{c-i\infty}^{c+\infty} \frac{d\omega}{2\pi i} \exp(\omega Y) F(\mathbf{r}_0, \mathbf{r}, \mathbf{b}; \omega), \tag{22}$$

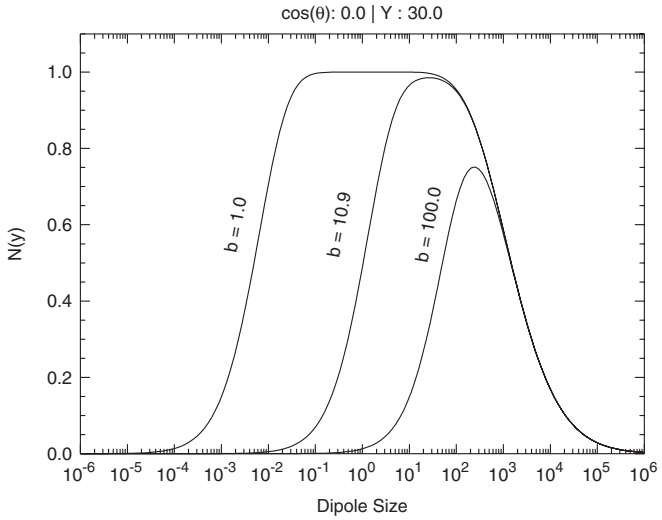

(a) Impact parameter dependent amplitude for the fixed coupling $\alpha_s = 0.1$ case as a function of the dipole size and for different values of the impact parameter.

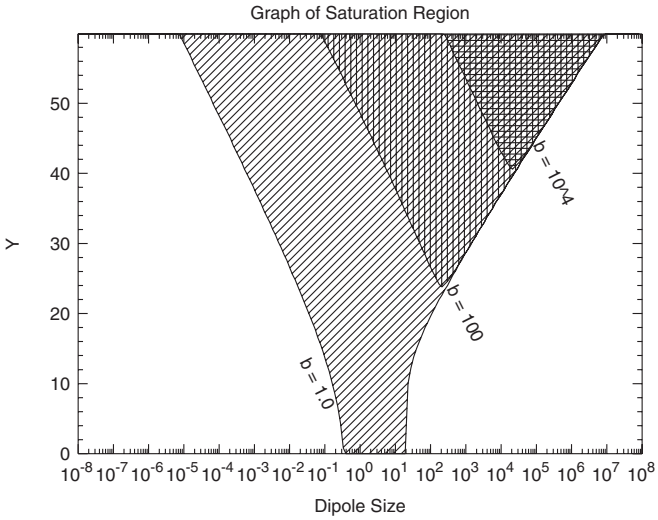

(b) Saturation region in $(Y, \ln r)$ plane for different impact parameters.

FIG. 12. (a) Impact parameter dependent amplitude for the fixed coupling $\alpha_s = 0.1$ case as a function of the dipole size and for different values of the impact parameter. (b) The saturation region in $(Y, \ln r)$ plane for different impact parameters.

with

$$F(\mathbf{r}_0, \mathbf{r}, \mathbf{b}; \omega) = \sum_{n=-\infty}^{+\infty} \int_{-\infty}^{\infty} d\nu \int d^2\mathbf{w} \left(\nu^2 + \frac{n^2}{4}\right) \times \frac{\mathcal{F}(\nu, n, \alpha_s; \omega)}{[\nu^2 + (\frac{n-1}{2})^2][\nu^2 + (\frac{n+1}{2})^2]} \times E^{n,\nu*}\left(\frac{\mathbf{r}_0}{2} - \mathbf{w}, -\frac{\mathbf{r}_0}{2} - \mathbf{w}\right) \times E^{n,\nu}\left(\frac{\mathbf{r}}{2} + \mathbf{b} - \mathbf{w}, -\frac{\mathbf{r}}{2} + \mathbf{b} - \mathbf{w}\right), \quad (23)$$

where $\mathbf{r}_0$ and $\mathbf{r}$ are the transverse sizes of two scattering objects (for example, onia) and $\mathbf{b}$ is their relative impact parameter.

The conformal eigenfunctions are defined as

$$E^{n,\nu}(\rho_{10}, \rho_{20}) = (-1)^n \left(\frac{\rho_{12}}{\rho_{10}\rho_{20}}\right)^h \left(\frac{\rho^*_{12}}{\rho^*_{10}\rho^*_{20}}\right)^{\bar{h}}, \quad (24)$$

where complex notation for the two-dimensional vectors (ρ_x, ρ_y) has been used:

$$\rho = \rho_x + i\rho_y, \qquad \rho^* = \rho_x - i\rho_y,$$

and where the conformal weights are

$$h = \frac{1-n}{2} + i\nu, \qquad \bar{h} = \frac{1-n}{2} + i\nu.$$

The function $\mathcal{F}(\nu, n, \alpha_s; \omega)$ contains the details of the dynamics. For the case of evolution with linear BFKL, the form of it is well known:

$$\mathcal{F}^{\mathrm{BFKL}}(\nu, n, \alpha_s; \omega) = \frac{1}{\omega - \chi(n, \nu)},$$

with

$$\chi(n, \nu) = 2\Psi(1) - \Psi\left(\frac{1 + |n|}{2} + i\nu\right) - \Psi\left(\frac{1 + |n|}{2} - i\nu\right)$$

being the LO BFKL kernel eigenvalue. In the case of the nonlinear equation the exact form of the function $\mathcal{F}(\nu, n, \alpha_s; \omega)$ is unknown. The origins of the peaks in the amplitude can be understood by analyzing the transverse structure encoded in functions $E^{n,\nu}$. We fix $\mathbf{r}_0$ and investigate the dependence on $\mathbf{r}$ from the transverse integral. We switch from the vector notation to the complex notation for the arguments of the E functions. Using the explicit expression (23) we obtain

$$\int d^2w E^{n,\nu*}\left(\frac{r_0}{2} - w, -\frac{r_0}{2} - w\right) E^{n,\nu}\left(\frac{r}{2} + b - w, -\frac{r}{2} + b - w\right) = \int d^2w E^{n,\nu*}\left(\frac{r_0}{2} - w, -\frac{r_0}{2} - w\right)(-1)^n \times \left(\frac{r}{(b + \frac{r}{2} - w)(b - \frac{r}{2} - w)}\right)^h \times \left(\frac{r^*}{(b + \frac{r}{2} - w)^*(b - \frac{r}{2} - w)^*}\right)^{\bar{h}}, \quad (25)$$

where we switched to the complex notation for the arguments. The biggest contribution comes from the region of $w \simeq 0$. For our purposes it is also enough to take $n = 0$. In this region the integrand has the approximate form

$$E^{n,\nu*}\left(\frac{r_0}{2},-\frac{r_0}{2}\right)\left(\frac{|r|^2}{[b^2-(\frac{r}{2})^2][(b^*)^2-(\frac{r^*}{2})^2]}\right)^{1/2+i\nu}. \quad (26)$$

Using $b=|b|e^{i\theta_b}$, $r=|r|e^{i\theta_r}$, and $\Delta\theta=\theta_r-\theta_b$ we have that

$$E^{n,\nu*}\left(\frac{r_0}{2},-\frac{r_0}{2}\right)\times\left(\frac{|r|^2}{[|b|^2-e^{2i\Delta\theta}(\frac{|r|}{2})^2][|b|^2-e^{-2i\Delta\theta}(\frac{|r|}{2})^2]}\right)^{1/2+i\nu}. \quad (27)$$

It is immediately clear that there will be angular dependence for the $b\simeq\frac{r}{2}$ case with the configurations of aligned dipoles $\Delta\theta=0,\pi$ giving the largest contributions. In the case of the perpendicular orientation of dipoles with respect to the impact parameter $\theta=\pi/2,-\pi/2$, the expression reduces to

$$E^{n,\nu*}\left(\frac{r_0}{2},-\frac{r_0}{2}\right)\left(\frac{|r|}{|b|^2+(\frac{|r|}{2})^2}\right)^{1+2i\nu}. \quad (28)$$

This structure is responsible for the presence of the peak in the amplitude in the case when b is fixed and r varied, and the absence of the peak in the case when r is fixed and b varied, for $\Delta\theta=\pi/2,-\pi/2$. This corresponds to the situations in the right-hand plots in Figs. 7 and 8, correspondingly.

An expression for the saturation scale dependent on the impact parameter can be derived using the method in [40]. To this aim one needs to take the Mellin representation for the solution to the linear equation and apply the absorptive boundary. The integral over the transverse variable can be performed using the representation [4]

$$\begin{aligned}\int d^2\rho_0 E^{n,\nu}(\rho_{10},\rho_{20})E^{n,\nu*}(\rho_{1'0},\rho_{2'0})&=c_1x^h x^{*\bar{h}}F(h,h,2h;x)F(\bar{h},\bar{h},2\bar{h};x^*)\\&+c_2x^{1-h}x^{*1-\bar{h}}F(1-h,1-h,2-2h;x)\\&\times F(1-\bar{h},1-\bar{h},2-2\bar{h};x^*),\end{aligned} \quad (29)$$

where

$$x=\frac{\rho_{12}\rho_{1'2'}}{\rho_{11'}\rho_{22'}} \quad (30)$$

is the anharmonic ratio and F are the hypergeometric functions. To obtain the saturation scale we take $n=0$ and expand around $x\simeq 0$. This simplifies the above expressions as in this limit $F(h,h,2h;x)\sim 1$ and the whole dependence on x comes through factors $x^h x^{*\bar{h}}$. In the case when the impact parameter b is much larger than the dipole sizes, $b\gg r, r_0$, one has

$$|x|\simeq\frac{rr_0}{b^2}.$$

Putting everything together, the scattering amplitude in the linear evolution case reduces to [65,66]

$$F(\mathbf{r}_0,\mathbf{r},\mathbf{b};Y)=-\frac{\alpha_s^2 r_0 r}{b^2}\int_{-\infty}^{\infty}\frac{d\nu}{2\pi}\frac{i\nu}{[\nu^2+\frac{1}{4}]^2}\times\exp\left(\bar{\alpha}_s\chi(\lambda)Y+2i\nu\ln\frac{b^2}{r_0 r}\right). \quad (31)$$

Here, we have taken into account the contribution from only zero conformal spin. Using $\lambda=1/2+i\nu$ the above expression can be recast into

$$F(\mathbf{r}_0,\mathbf{r},\mathbf{b};Y)=-\alpha_s^2\int_{(1/2)-i\infty}^{(1/2)+i\infty}\frac{d\lambda}{2\pi}2(\lambda-1/2)\times\exp\left(\bar{\alpha}_s\chi(\lambda)Y-(1-\lambda)\ln\left(\frac{b^2}{r_0 r}\right)^2\right), \quad (32)$$

where the prefactor in (31) has been expanded around $\nu=0$. Taking the saddle point condition and the condition that the exponent vanishes at the saddle point which is the requirement on the saturation boundary one arrives at two conditions for this line (noted by a subscript 0):

$$\bar{\alpha}_s Y\chi'(\lambda_0)+\ln(b^2/(r_0 r))^2=0, \quad (33)$$

$$\bar{\alpha}_s Y\chi(\lambda_0)-(1-\lambda_0)\ln(b^2/(r_0 r))^2=0. \quad (34)$$

These equations can be solved to yield the saturation scale but it was found that one can include further corrections [40]. We can obtain these corrections by using the solution to the saddle point equation to find λ_c and use this to evaluate the prefactor. The resulting modified equations are then

$$\bar{\alpha}_s Y\chi'(\lambda_c)+\ln(b^2/(r_0 r))^2=0, \quad (35)$$

$$\bar{\alpha}_s Y\chi(\lambda_c)-(1-\lambda_c)\ln(b^2/(r_0 r))^2=\tfrac{3}{2}\ln[\bar{\alpha}_s Y\chi''(\lambda_c)]. \quad (36)$$

By keeping one of the dipole sizes fixed, say, r_0, we can solve for r to get the saturation line

$$Q_{c,1}^2(r_0,b;Y)=\frac{r_0^2}{b^4}\frac{e^{\bar{\alpha}_s Y\chi(\lambda_c)/(1-\lambda_c)}}{[\bar{\alpha}_s Y\chi''(\lambda_c)]^{3/2(1-\lambda_c)}}. \quad (37)$$

For large $\bar{\alpha}_s Y$ the λ_c approaches the λ_0 value, with $\lambda_0=0.37$. The saturation scale has $1/b^4$ dependence, which comes automatically from conformal symmetry. One can solve the above equation for b and keep r_0 and r fixed, which yields

$$B_s^2(r_0,r;Y)=r_0 r\frac{e^{\bar{\alpha}_s Y\chi(\lambda_c)/2(1-\lambda_c)}}{[\bar{\alpha}_s Y\chi''(\lambda_c)]^{3/4(1-\lambda_c)}}. \quad (38)$$

This is the rate of the expansion of the radius in impact parameter space. Note that the speed of the expansion is governed by the exponent which is half that of the saturation scale and the dependence on the dipole size is linear.

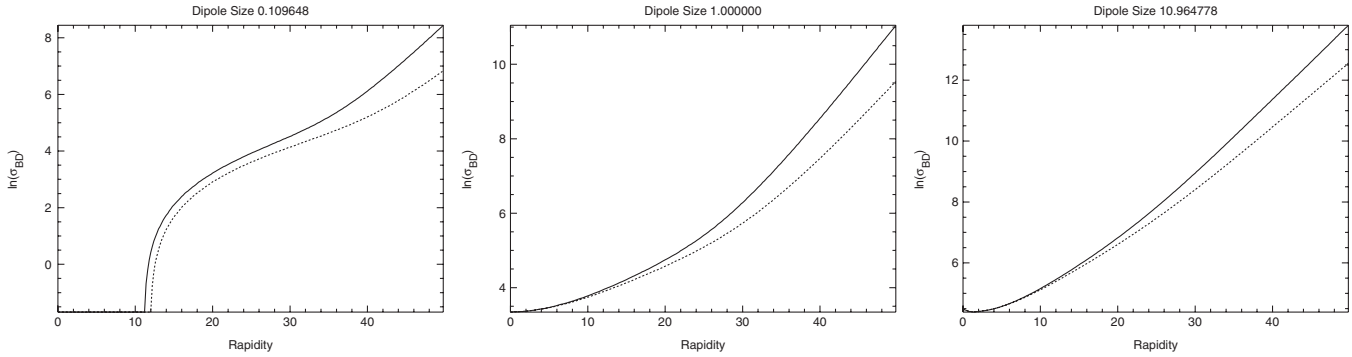

(a) $r = 0.11$ (b) $r = 1.0$ (c) $r = 11.0$

FIG. 13. Graphs of the natural logarithm of the black disk cross section versus rapidity at various fixed dipole sizes. The dashed line represents the solutions obtained with the Bessel kernel, while the solid line represents the solutions with the LO kernel.

This is also found in the numerical solution. For the large dipole sizes $r \gg r_0, b$ the anharmonic ratio reduces to

$$|x| \simeq \frac{4r_0}{r}.$$

Following the same scheme one obtains for the saturation scale

$$Q_{c,2}^2(r_0, b; Y) = \frac{e^{\bar{\alpha}_s Y \chi(\lambda_c)/(1-\lambda_c)}}{r_0^2[\bar{\alpha}_s Y \chi''(\lambda_c)]^{3/2(1-\lambda_c)}}. \quad (39)$$

The saturation scale for large dipole sizes is independent of the impact parameter b. This is also found in the solution, as is clear in Fig. 12. Therefore the V shape of the saturation region is a consequence of the conformal symmetry of the LO kernel. From the above considerations one can see that the rapidity behavior of both saturation scales is identical for large and small dipoles. We found that the two exponents differ somewhat; see Table I. Most probably this is due to the fact that we have neglected an additional angle which is necessary to fully describe the orientation of the dipoles. In this solution here, one is taking the angular average over the spatial configurations of the dipoles which can result in a slightly faster expansion in impact parameter space. However, a more detailed analysis is needed to confirm this effect.

In general we see that both saturation scales are in fact originating from one saturation scale due to the fact that the solution is expressed in terms of the anharmonic ratio.

E. Dipole cross section and black disk radius

By integrating the amplitude over the impact parameter the dipole cross section is obtained as a function of the dipole size and rapidity. Despite the fact that the amplitude is bound and never exceeds unity, the dipole cross section can still increase very fast due to the fact that the amplitude has power tails in the impact parameter; see the discussion in [67,68]. We thus expect the powerlike growth of the dipole cross section with the energy or exponential with rapidity.

The dipole cross section is defined as an integral over b of the amplitude

$$\sigma(r, Y) = 2 \int d^2\mathbf{b} N(\mathbf{r}, \mathbf{b}, Y). \quad (40)$$

In what follows, we will investigate the part of the dipole cross section which is coming from the black disk regime. To be precise, we integrate the amplitude over the values which are close to unity. This is once again performed by constraining the amplitude through Eq. (19).

The black disk (BD) part of the cross section is therefore defined as

$$\sigma_{\mathrm{BD}}(r, Y) = 2 \int d^2\mathbf{b} N(\mathbf{r}, \mathbf{b}, Y) \Theta[N(\mathbf{r}, \mathbf{b}, Y) - \kappa]$$
$$\approx 2\pi R_{\mathrm{BD}}^2(r, Y). \quad (41)$$

This black disk cross section is plotted in Fig. 13, and it can be seen that the slope of the black disk cross section in rapidity reaches a constant value at large rapidities. One can parametrize R_{BD} as

$$R_{\mathrm{BD}}^2(r, Y) = R_{\mathrm{BD}}^{(0)2} e^{\lambda_{\mathrm{BD}} \bar{\alpha}_s Y}, \quad (42)$$

where $R_{\mathrm{BD}}^{(0)}$ is a normalization constant and λ_{BD} is extracted from the numerical solutions in the regime where it is approximately constant. These extracted values for the solutions with two kernels as well as various values of $\bar{\alpha}_s$ are found in Table II. The table also shows that with changing $\bar{\alpha}_s$ the exponent is relatively constant for the LO kernel, and once again nonlinearities in the exponent

TABLE II. Extracted exponents governing the behavior of the black disk cross section.

	λ_{BD}
LO kernel $\bar{\alpha}_s = 0.1$	2.4
Modified kernel $\bar{\alpha}_s = 0.1$	2.0
LO kernel $\bar{\alpha}_s = 0.2$	2.6
Modified kernel $\bar{\alpha}_s = 0.2$	1.6

appear for the Bessel kernel. Reported exponents are averaged from values of dipole size $r = 10^{-1} \rightarrow 10^{1}$ because λ_{BD} does vary slightly with dipole size.

VI. INCLUDING THE RUNNING COUPLING

Turning now to the running of the QCD coupling, $\bar{\alpha}_s$ is taken to be $\alpha_s(r) = 1/b \ln(\frac{1}{r^2\lambda^2})$ where $b = \frac{33-2n_f}{12\pi}$, n_f is the number of active flavors and $\lambda = 0.246$ GeV is used. In the infrared regime, the coupling was frozen when $r > r_{\mathrm{cut}}$, which is defined as $\bar{\alpha}_s(r_{\mathrm{cut}}) = 0.3$. As is well known the BK equation without the impact parameter is not very sensitive to the way the coupling is regularized. This is because the amplitude is saturated for all the large values of the dipole size from the inverse of the saturation scale to infinity. In the case with the impact parameter, however, there are contributions from the large dipole regime which spoil this self-regularizing behavior. In this case there is a large sensitivity to the regularization scenario for the running coupling.

There are two different schemes for including the running coupling in the BK equation [69,70]. In addition to these two scenarios we will use also the so-called parent dipole scheme, where the coupling depends on the size of the external dipole, that is, x_{01}. This scheme is convenient to use with the Bessel function kernel. We have also evaluated the solutions using the prescription proposed in [69]:

$$K^{\mathrm{Bal}}(x_{01}, x_{02}) = \frac{N_c \alpha_s(x_{01}^2)}{2\pi^2}\left[\frac{x_{01}^2}{x_{02}^2 x_{12}^2} + \frac{1}{x_{02}^2}\left(\frac{\alpha_s(x_{02}^2)}{\alpha_s(x_{12}^2)} - 1\right) + \frac{1}{x_{12}^2}\left(\frac{\alpha_s(x_{12}^2)}{\alpha_s(x_{02}^2)} - 1\right)\right]. \quad (43)$$

Since it is not clear at the moment how to use this scheme with the Bessel function kernel we will use it only with the LO kernel. The scheme dependence between the two prescriptions [69,70] originates from the choice of the subtraction point. The scheme by Ref. [70] was shown to agree with the scheme by Ref. [69] by the calculation of the appropriate subtraction corrections. In this paper we have not evaluated the scheme by Ref. [70], as we have found that in order to achieve the desired accuracy for the solution with the impact parameter within this scheme takes considerably longer time.

We first shall show the results with the running coupling without the impact parameter. The running of the coupling has the effect of slowing down the evolution of the scattering amplitude as seen in Fig. 14. The difference between the LO and the modified kernel with the running coupling is rather small. This can also be seen in Fig. 15, which shows the saturation scale of the two kernels with the running coupling which are extremely close to each other. The dependence on the saturation scale with respect to the rapidity is as in Refs. [40,57]:

$$Q_s^2 = \lambda^2 \exp\left[\left(\frac{2\chi(\gamma_c)}{b\gamma_c} Y\right)^{1/2} + \frac{3}{4}\xi_1\left(\frac{\chi''(\gamma_c)}{2b\gamma_c\chi(\gamma_c)}\right)^{1/3} Y^{1/6}\right], \quad (44)$$

where $\xi_1 = -2.338$. Here the second term involving $Y^{1/6}$ is numerically non-negligible for the rapidities we consider. In terms of numbers the coefficients above give $Q_s^2 = \lambda^2 e^{3.6Y^{1/2} - 5.4Y^{1/6}}$. We have found that the LO saturation scale with the running coupling and the parent dipole

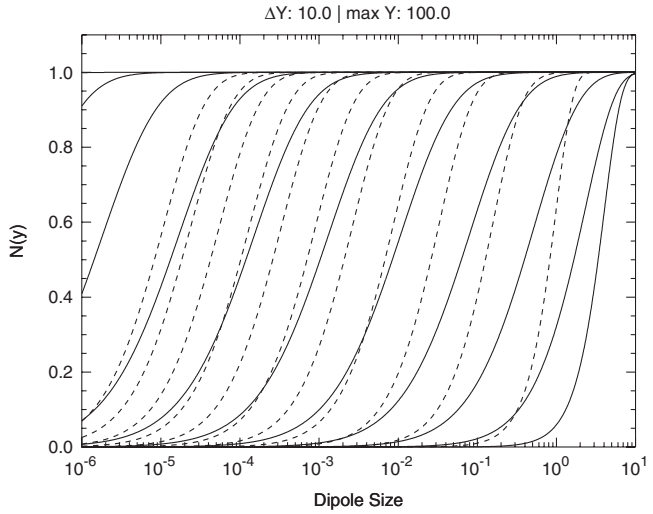

(a) Solid line: LO kernel with fixed $\bar{\alpha}_s = 0.1$; dashed line: LO kernel with $\bar{\alpha}_s = \bar{\alpha}_s(r)$

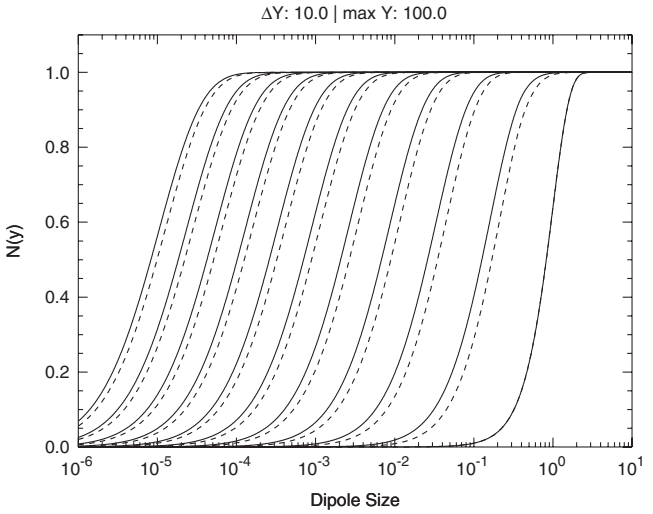

(b) Solid line: LO kernel with $\bar{\alpha}_s = \bar{\alpha}_s(r)$; dashed line: modified kernel $\bar{\alpha}_s = \bar{\alpha}_s(r)$

FIG. 14. Graphs of the scattering amplitude versus the dipole size for the case without the impact parameter. The left graph illustrates how much slower propagation is due to the running of the coupling, and the right graph shows the modified and LO kernels compared to each other in the case of the running coupling. Each line corresponds to the rapidity increasing in rapidity in intervals of $\Delta Y = 10$ up to $Y = 100$.

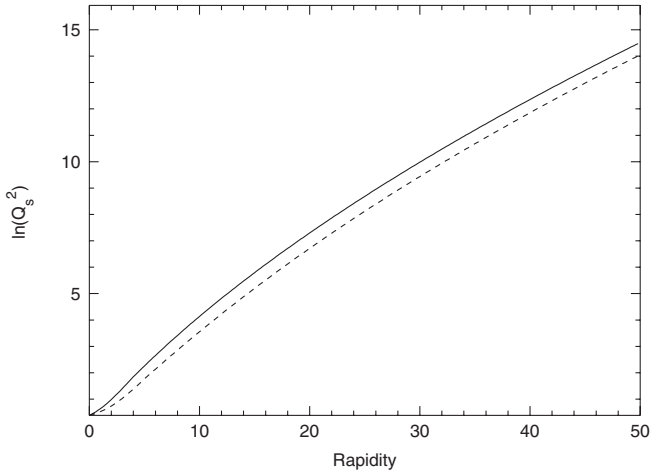

FIG. 15. Graph of the saturation scale of the LO kernel (solid line) and the modified kernel (dashed line) with running coupling and no impact parameter dependence.

size prescription is $Q_s^2 = e^{3.4Y^{1/2}-4.8Y^{1/6}}$, which is very similar to the one given by the analytical value. The running coupling with prescription (43) has also been run and found to have a fit of $Q_s^2 = e^{3.4Y^{1/2}-5.7Y^{1/6}}$, which is closer to the value given by (44).

In the scenario with the impact parameter we find quite different behavior of the solution. As is seen in Fig. 16(a) the evolution of the running coupling (with the parent dipole scheme) is actually very fast in the small dipole region, and it is much faster in the large dipole region. This is obvious since in the large dipole region the coupling is fixed at $\bar{\alpha}_s = 0.3$, which yields approximately 3 times as fast an evolution versus the case where $\bar{\alpha}_s = 0.1$ is fixed. It can be seen there are box effects beginning to manifest in the running coupling case due to the frozen coupling evolving very quickly in the large dipole regime and reaching the box.

It can be seen in Fig. 17 that the dependence of the saturation scales on the rapidity is now again almost exponential. In this case we can extract the exponents by fitting exponential forms in the rapidity as we did for the fixed coupling case (Table III). Note that the definitions of the exponents are now different than in the previous section. Here, we took $Q_s \sim \exp(\lambda_s Y)$, $Q_{sL} \sim \exp(-\lambda_L Y)$, and $B_s \sim \exp(\lambda_B Y)$. The reason that the dependencies are almost exponential is due to the large sensitivity to the infrared and the fact that the coupling is frozen. In that case the solutions behave almost as with the fixed running determined by the freezing value.

A similar pattern is found in the case of the running coupling with the scenario (43). The only difference is in the small dipole regime where the evolution is slightly slower than that of the parent dipole scheme. This can be seen by comparing the extracted exponents in Table III.

The behavior observed is of course something that has been analyzed before, in the context of the linear BFKL with running coupling [71]. In particular, it was observed that the BFKL solution shows the tunneling scenario, where at some value of rapidity the solution is completely dominated by the infrared region. Strictly speaking we are not observing the tunneling scenario here, due to the fact that we have chosen our initial conditions to be concentrated around rather large dipole sizes where the coupling is already large.

Rather, our solutions are completely dominated by the large coupling values and hence the saturation scale has

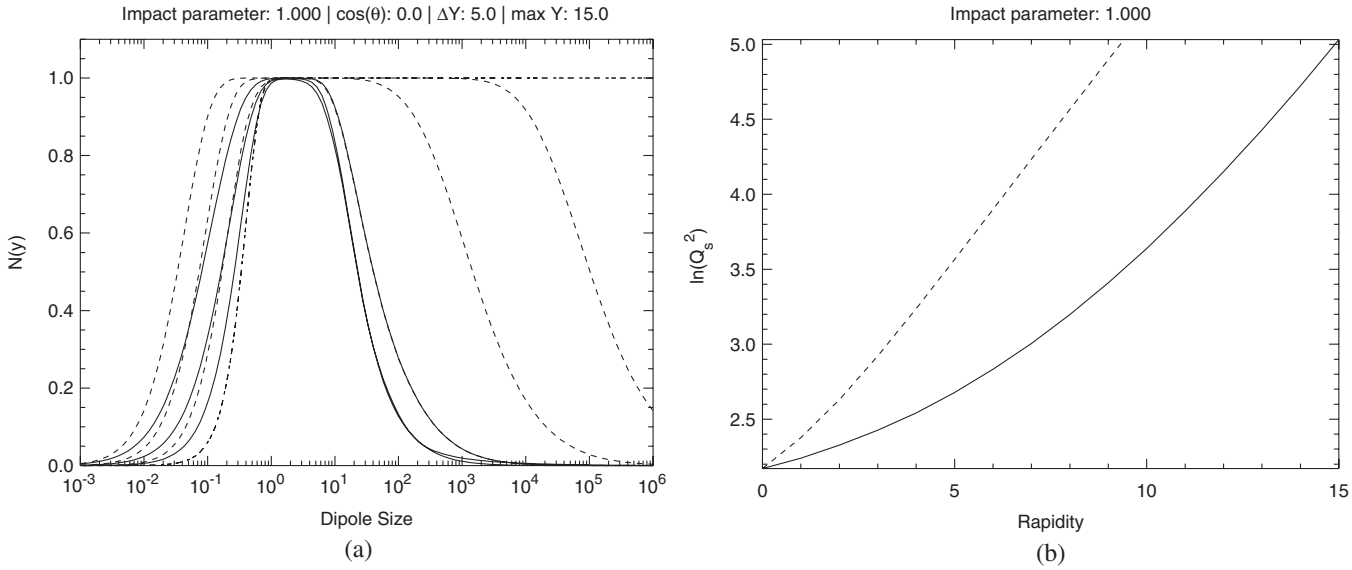

FIG. 16. (a) Dipole scattering amplitude as a function of the dipole size for the fixed impact parameter and angle. Solid lines: Fixed coupling with $\bar{\alpha}_s = 0.1$; dashed lines: running coupling with the parent dipole scheme. (b) Saturation scale as a function of rapidity for the LO kernel, the fixed coupling $\bar{\alpha}_s = 0.1$ (solid line) and running coupling (dashed line) cases.

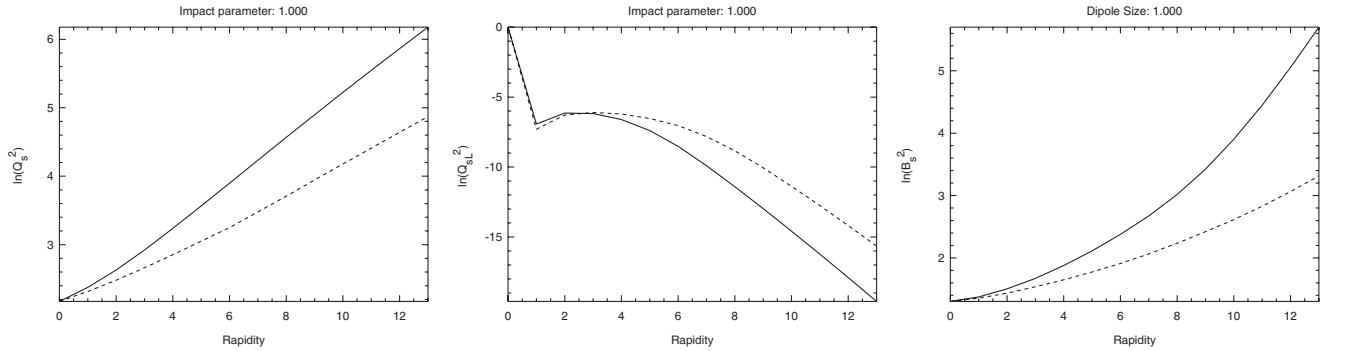

(a) Saturation scale at small dipole size (b) Saturation scale at large dipole size (c) Black disc radius in impact parameter

FIG. 17. Small dipole saturation scale, large dipole saturation scale, and the black disk radius for the case of the running coupling within the parent dipole scheme. The solid lines are for the LO kernel, and the dashed lines are for Bessel kernel.

nearly exponential dependence on rapidity. It will be interesting to analyze the solution for the initial conditions which are located in the small dipole regime to see if the tunneling occurs here.

We have also evaluated the dipole cross section coming from the black disk regime in the running coupling scenario, and we parametrize it in the form

$$\sigma_{\mathrm{BD}} = 2\pi R_{\mathrm{BD}}^2(x, Y) = 2\pi R_{\mathrm{BD}}^{(0)2} e^{\lambda_{\mathrm{BD}} Y}. \tag{45}$$

The extracted value for the exponent λ_{BD} is shown also in Table III. Again the black disk cross section increases very fast due to the large value of the coupling in the region of freezing. We have also compared the solutions in the case of the LO and Bessel kernel; the results are shown in Fig. 18. Since the coupling is relatively large, the differences between the evolution with LO and Bessel kernels are more amplified.

The anomalous dimension

We have also extracted from the numerical solution the value of the anomalous dimension defined by the parametrization $N \sim r^{2\gamma_s}$. In the impact parameter dependent case one has two anomalous dimensions, the second one for the large dipole sizes, which we parametrize as $N \sim r^{-2\gamma_l}$. The extracted values of the anomalous dimension for the different scenarios are summarized in Table IV. The values of the anomalous dimension change significantly depending on the value of the amplitude at which they were extracted.

TABLE III. Summary of extracted evolution exponents with the impact parameter for the running coupling case. PD means parent dipole prescription, and Bal means prescription (43).

	λ_s	λ_L	λ_B	λ_{BD}
LO kernel $\bar{\alpha}_s^{(\mathrm{PD})}$	0.30	1.68	0.60	0.65
LO kernel $\bar{\alpha}_s^{(\mathrm{Bal})}$	0.29	1.68	0.64	0.68
Bessel kernel $\bar{\alpha}_s^{(\mathrm{PD})}$	0.22	1.42	0.24	0.32

Therefore the range of values of the amplitude is shown which gives the corresponding range of values of the anomalous dimension.

To illustrate better the variation of the anomalous dimension on the rapidity and the dipole size we have plotted the extracted effective anomalous dimension defined by $\gamma^{\mathrm{eff}} \equiv \frac{\partial \ln N}{\partial \ln r}$ as a function of the scaling variable rQ_s for different values of rapidity. This is shown in Fig. 19, where in the left plot we show the calculation in the fixed coupling case and on the right-hand side for the running coupling case. The geometrical scaling is observed when the curves of different rapidity coincide with each other.[1] The anomalous dimension clearly exhibits a change in the dependence on the scaling variable. Roughly speaking the change in the extracted anomalous dimension coincides with the size of the scaling window. The change appears at about $\gamma \sim 0.5$–0.6, which is relatively consistent with the analytical estimates [40]. The scaling is much better in the fixed coupling case than in the running coupling case.

In the impact parameter dependent case the anomalous dimensions for the fixed coupling LO case are about the same as in the impact parameter independent scenario. The anomalous dimension in the running coupling case is also close to the one in the impact parameter independent solution. On the other hand, the cutoffs induced by the modification of the kernel result in the larger anomalous dimension in the impact parameter dependent scenario, and this is quite different from the local solution. We also note that in the case of the Bessel kernel there is a dependence on the value of the fixed coupling at which the anomalous dimension is extracted, meaning that the corrections are nonlinear in the coupling.

The anomalous dimension for the larger dipoles turns out to be slightly lower, of about $\gamma_l \sim 0.58$–0.6, and the

[1]The sharp rise of the anomalous dimension at the left edges of the curves is not physical but rather an artifact of the numerical effect, the value of the amplitude in this region is very small, and the numerical errors tend to be rather large.

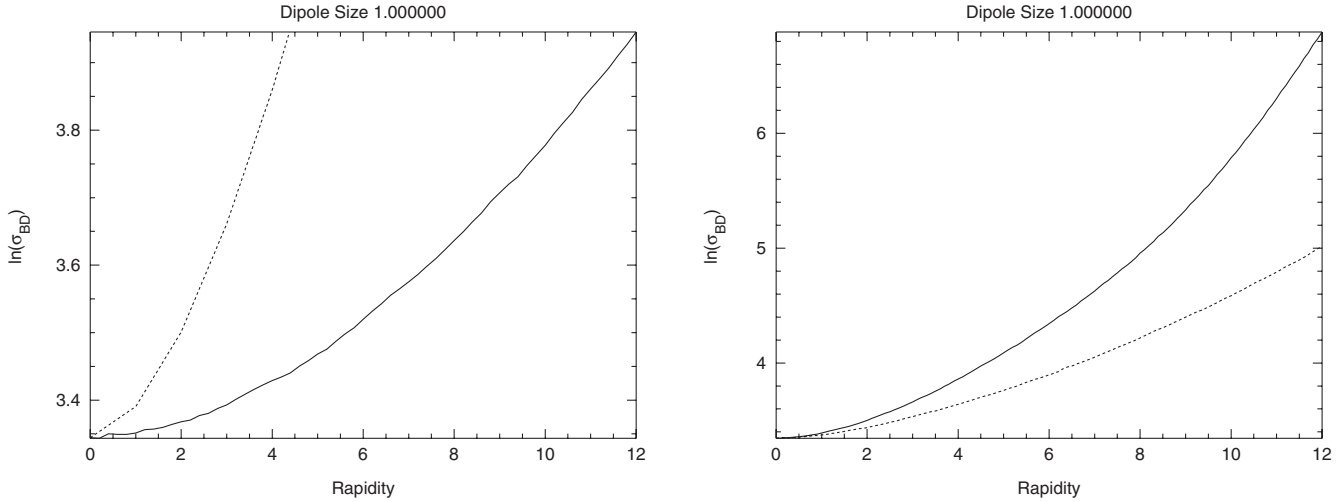

(a) Black disc cross section for the fixed coupling $\alpha_s = 0.1$ case (solid line) versus the running coupling case (dashed line), both for the LO kernel

(b) Black disc cross section for case of running coupling with the LO kernel (solid line) versus the running coupling case with the Bessel kernel(dashed line)

FIG. 18. Dipole cross section. Contribution from the "black disk."

variations among the scenarios are not significant with respect to the accuracy of the solution. From arguments of conformal symmetry one would think that the value of γ_l should be the same in the LO fixed coupling case as γ_s. One reason for that could be that one is extracting these values at different values of rapidity; this is in order to avoid the dependencies of the finite extension of the grid one is working with. In this case the typical rapidities are smaller and therefore the anomalous dimension can be systematically lower as well (this is seen in the case of γ_s). The second reason could be that one is using the assumption of the independence of the solution on the global azimuthal angle which possibly leads to small violations of the conformal symmetry. We observe though that the values of γ_l are comparable for different scenarios. This has a rather clear explanation, as the running coupling should not affect the γ_l since it is regularized in this region, and therefore the solution for large dipole sizes with the running coupling should have the same characteristics as in the fixed coupling case. The fact that the modified Bessel function kernel is not affecting large dipole sizes is also consistent with the arguments presented in Sec. V C. Clearly these results call for more extensive analytical and numerical studies.

TABLE IV. Extracted values of the anomalous dimension in different scenarios. Y_s and Y_l are the rapidities at which the exponents were extracted. N range means the range of values of the amplitude for which the values were computed.

With impact parameter dependence	N range	Y_s	γ_s	Y_l	γ_l
LO kernel $\bar{\alpha}_s = 0.1$	$10^{-4} \to 10^{-2}$	40	$0.68 \to 0.58$	30	$0.58 \to 0.47$
Bessel kernel $\bar{\alpha}_s = 0.1$	$10^{-4} \to 10^{-2}$	50	$0.77 \to 0.66$	30	$0.58 \to 0.46$
LO kernel $\bar{\alpha}_s = 0.2$	$10^{-4} \to 10^{-2}$	20	$0.67 \to 0.59$	15	$0.60 \to 0.46$
Bessel kernel $\bar{\alpha}_s = 0.2$	$10^{-4} \to 10^{-2}$	25	$0.90 \to 0.77$	15	$0.56 \to 0.47$
LO kernel $\bar{\alpha}_s =$ run (parent dipole)	$10^{-4} \to 10^{-2}$	17	$0.86 \to 0.77$	8	$0.60 \to 0.49$
LO kernel $\bar{\alpha}_s =$ run (Balitsky)	$10^{-4} \to 10^{-2}$	13	$0.87 \to 0.79$	9	$0.57 \to 0.47$
Bessel kernel $\bar{\alpha}_s =$ run (parent dipole)	$10^{-4} \to 10^{-2}$	13	$1.15 \to 1.02$	8	$0.58 \to 0.47$
No impact parameter dependence					
LO kernel $\bar{\alpha}_s = 0.1$	$10^{-6} \to 10^{-2}$	60	$0.68 \to 0.55$	X	X
Bessel kernel $\bar{\alpha}_s = 0.1$	$10^{-6} \to 10^{-2}$	60	$0.68 \to 0.55$	X	X
LO kernel $\bar{\alpha}_s = 0.2$	$10^{-4} \to 10^{-2}$	40	$0.68 \to 0.54$	X	X
Bessel kernel $\bar{\alpha}_s = 0.2$	$10^{-4} \to 10^{-2}$	40	$0.64 \to 0.55$	X	X
LO kernel $\bar{\alpha}_s =$ run (parent dipole)	$10^{-6} \to 10^{-2}$	100	$0.82 \to 0.67$	X	X
LO kernel $\bar{\alpha}_s =$ run (Balitsky)	$10^{-6} \to 10^{-2}$	100	$0.81 \to 0.67$	X	X
Bessel kernel $\bar{\alpha}_s =$ run (parent dipole)	$10^{-6} \to 10^{-2}$	100	$0.82 \to 0.67$	X	X

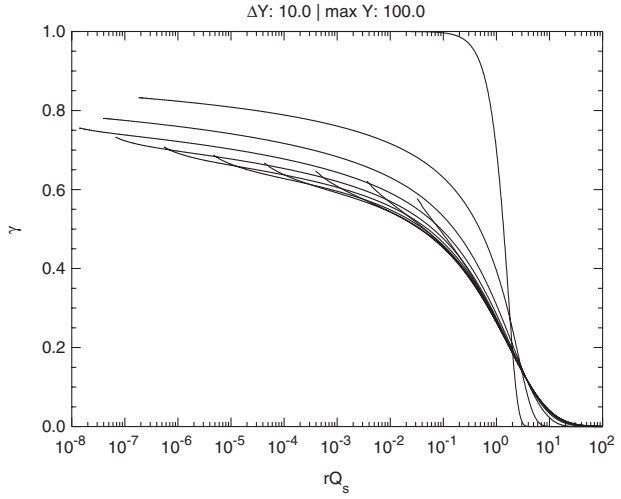

(a) Anomalous dimension for the fixed coupling $\alpha_s = 0.1$ case for LO kernel as a function of the scaling variable. Curves correspond to different values of rapidity, starting from $Y = 0$ to $Y = 100$ in $\Delta Y = 10$ intervals.

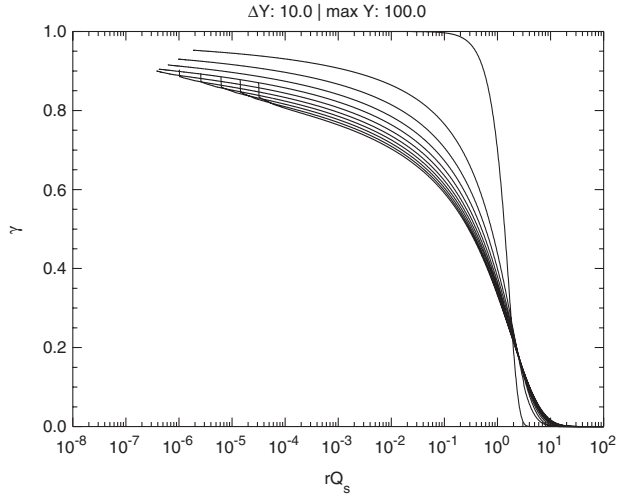

(b) Anomalous dimension for the running coupling case for LO kernel as a function of the scaling variable. Curves correspond to different values of rapidity, starting from $Y = 0$ to $Y = 100$ in $\Delta Y = 10$ intervals.

FIG. 19. Anomalous dimension for the solution to the BK equation without impact parameter dependence.

VII. CONCLUSIONS

Let us summarize the most important points of our analysis.

In the case of the solution with the LO kernel, the extracted exponents of the saturation scales and the black disk radius are consistent with values obtained from the boundary method. The peaks in the impact parameter and in the dipole size can be very easily understood from arguments based on the conformal symmetry. The relative strength of the evolution of different saturation scales follows as well from the arguments on the conformal symmetry. In particular, the black disk radius has an expansion rate which is twice slower than that of the saturation scale for small dipoles (as we mentioned before, this is only approximately true due to effects of angular averaging).

For the running coupling scenario, in the case of the solutions with the impact parameter we no longer observe the self-regularizing behavior of the nonlinear equation. This is of course due to the increased sensitivity to the large values of the dipole size. Rather, for the initial conditions chosen one observes strong dependence on the details of the regularization, and basically the exponents of both the saturation scales are dominated by the largest value of the coupling. This could be tested in more detail by choosing a different initial condition; nevertheless one can expect that for the sufficiently large rapidity, the solution becomes regularization-sensitive, much like it was observed in earlier simulations.

The cuts on the large dipole sizes introduced in the form of the modified kernel have in general a very small effect for the case of the impact parameter independent kernel. For the case with the impact parameter they are no longer negligible and reduce the exponent by about 25% for coupling of $\bar{\alpha}_s = 0.1$. It is important to note that the modified kernel we have chosen does not account for all the type of kinematical cuts, and therefore other cuts on the small dipole sizes should be included similarly to what was done in [53]. One could expect therefore an even stronger effect in this case.

We therefore conclude that the observed self-regularizing behavior of the local BK equation with the running coupling and almost complete insensitivity to the other next-to-leading-order corrections probably appear due to the simplified assumption about the impact parameter independence.

In a broader perspective, it will be interesting to perform the analysis with a full next-to-leading-order kernel or the more correct form of the kinematical cuts, as well as to introduce effectively confinement effects. It is also vital to analyze the impact of the corrections which go beyond the mean field approximation [66,72–74].

ACKNOWLEDGMENTS

We thank Emil Avsar and Leszek Motyka for interesting discussions. This work was supported by MNiSW Grant No. N202 249235 and the DOE OJI Grant No. DE - SC0002145. A. M. S. is supported by the Sloan Foundation.

[1] V. S. Fadin, E. A. Kuraev, and L. N. Lipatov, Phys. Lett. **60B**, 50 (1975).
[2] E. A. Kuraev, L. N. Lipatov, and V. S. Fadin, Sov. Phys. JETP **45**, 199 (1977).
[3] I. I. Balitsky and L. N. Lipatov, Sov. J. Nucl. Phys. **28**, 822 (1978).
[4] L. N. Lipatov, Sov. Phys. JETP **63**, 904 (1986).
[5] V. S. Fadin and L. N. Lipatov, Nucl. Phys. **B477**, 767 (1996).
[6] V. S. Fadin, M. I. Kotsky, and L. N. Lipatov, arXiv:hep-ph/9704267.
[7] V. S. Fadin and L. N. Lipatov, Phys. Lett. B **429**, 127 (1998).
[8] V. S. Fadin, M. I. Kotsky, and L. N. Lipatov, Phys. Lett. B **415**, 97 (1997).
[9] G. Camici and M. Ciafaloni, Phys. Lett. B **386**, 341 (1996).
[10] G. Camici and M. Ciafaloni, Phys. Lett. B **395**, 118 (1997).
[11] G. Camici and M. Ciafaloni, Phys. Lett. B **412**, 396 (1997).
[12] G. Camici and M. Ciafaloni, Nucl. Phys. B, Proc. Suppl. **54**, 155 (1997).
[13] M. Ciafaloni and G. Camici, Phys. Lett. B **430**, 349 (1998).
[14] L. V. Gribov, E. M. Levin, and M. G. Ryskin, Phys. Rep. **100**, 1 (1983).
[15] Y. V. Kovchegov, Phys. Rev. D **60**, 034008 (1999).
[16] Y. V. Kovchegov, Phys. Rev. D **61**, 074018 (2000).
[17] A. H. Mueller, Nucl. Phys. **B415**, 373 (1994).
[18] I. Balitsky, Nucl. Phys. **B463**, 99 (1996).
[19] I. Balitsky, Phys. Rev. Lett. **81**, 2024 (1998).
[20] I. Balitsky, Phys. Rev. D **60**, 014020 (1999).
[21] I. Balitsky, Phys. Lett. B **518**, 235 (2001).
[22] I. I. Balitsky and A. V. Belitsky, Nucl. Phys. **B629**, 290 (2002).
[23] J. Jalilian-Marian, A. Kovner, and H. Weigert, Phys. Rev. D **59**, 014015 (1998).
[24] J. Jalilian-Marian, A. Kovner, A. Leonidov, and H. Weigert, Phys. Rev. D **59**, 014014 (1998).
[25] E. Iancu, A. Leonidov, and L. D. McLerran, Nucl. Phys. **A692**, 583 (2001).
[26] E. Iancu, A. Leonidov, and L. D. McLerran, Phys. Lett. B **510**, 133 (2001).
[27] E. Ferreiro, E. Iancu, A. Leonidov, and L. McLerran, Nucl. Phys. **A703**, 489 (2002).
[28] H. Weigert, Nucl. Phys. **A703**, 823 (2002).
[29] A. H. Mueller, Phys. Lett. B **523**, 243 (2001).
[30] J. Bartels, Z. Phys. C **60**, 471 (1993).
[31] J. Bartels and M. Wusthoff, Z. Phys. C **66**, 157 (1995).
[32] J. Bartels, L. N. Lipatov, and G. P. Vacca, Nucl. Phys. **B706**, 391 (2005).
[33] M. Lublinsky, Eur. Phys. J. C **21**, 513 (2001).
[34] M. Lublinsky, E. Gotsman, E. Levin, and U. Maor, Nucl. Phys. **A696**, 851 (2001).
[35] K. J. Golec-Biernat, L. Motyka, and A. M. Stasto, Phys. Rev. D **65**, 074037 (2002).
[36] N. Armesto and M. A. Braun, Eur. Phys. J. C **20**, 517 (2001).
[37] M. A. Braun, arXiv:hep-ph/0101070.
[38] J. L. Albacete, N. Armesto, J. G. Milhano, C. A. Salgado, and U. A. Wiedemann, Phys. Rev. D **71**, 014003 (2005).
[39] J. L. Albacete and Y. V. Kovchegov, Phys. Rev. D **75**, 125021 (2007).
[40] A. H. Mueller and D. N. Triantafyllopoulos, Nucl. Phys. **B640**, 331 (2002).
[41] D. N. Triantafyllopoulos, Nucl. Phys. **B648**, 293 (2003).
[42] J. Bartels and K. Kutak, Eur. Phys. J. C **53**, 533 (2008).
[43] J. Bartels, L. N. Lipatov, and M. Wusthoff, Nucl. Phys. **B464**, 298 (1996).
[44] K. J. Golec-Biernat and A. M. Stasto, Nucl. Phys. **B668**, 345 (2003).
[45] E. Gotsman, M. Kozlov, E. Levin, U. Maor, and E. Naftali, Nucl. Phys. **A742**, 55 (2004).
[46] L. Motyka and A. M. Stasto, Phys. Rev. D **79**, 085016 (2009).
[47] J. Kwiecinski, A. D. Martin, and P. J. Sutton, Z. Phys. C **71**, 585 (1996).
[48] A. Kormilitzin and E. Levin, Nucl. Phys. **A849**, 98 (2011).
[49] G. Chachamis, M. Lublinsky, and A. Sabio Vera, Nucl. Phys. **A748**, 649 (2005).
[50] I. Balitsky and G. A. Chirilli, Phys. Rev. D **77**, 014019 (2008).
[51] E. Avsar, G. Gustafson, and L. Lonnblad, J. High Energy Phys. 01 (2007) 012.
[52] I. Balitsky and G. A. Chirilli, Phys. Lett. B **687**, 204 (2010).
[53] E. Avsar, G. Gustafson, and L. Lonnblad, J. High Energy Phys. 07 (2005) 062.
[54] A. H. Mueller, Nucl. Phys. **B558**, 285 (1999).
[55] A. H. Mueller, arXiv:hep-ph/9911289.
[56] C. Marquet and G. Soyez, Nucl. Phys. **A760**, 208 (2005).
[57] S. Munier and R. B. Peschanski, Phys. Rev. D **69**, 034008 (2004).
[58] G. P. Salam, J. High Energy Phys. 07 (1998) 019.
[59] M. Ciafaloni, D. Colferai, G. P. Salam, and A. M. Stasto, Phys. Rev. D **68**, 114003 (2003).
[60] A. Sabio Vera, Nucl. Phys. **B722**, 65 (2005).
[61] M. Ciafaloni, D. Colferai, and G. P. Salam, Phys. Rev. D **60**, 114036 (1999).
[62] E. Avsar, Acta Phys. Pol. B **37**, 3561 (2006).
[63] E. Avsar, J. High Energy Phys. 11 (2007) 027.
[64] M. Ryskin (unpublished).
[65] H. Navelet and S. Wallon, Nucl. Phys. **B522**, 237 (1998).
[66] Y. Hatta and A. H. Mueller, Nucl. Phys. **A789**, 285 (2007).
[67] A. Kovner and U. A. Wiedemann, Phys. Lett. B **551**, 311 (2003).
[68] A. Kovner and U. A. Wiedemann, Phys. Rev. D **66**, 051502 (2002).
[69] I. Balitsky, Phys. Rev. D **75**, 014001 (2007).
[70] Y. V. Kovchegov and H. Weigert, Nucl. Phys. **A784**, 188 (2007).
[71] M. Ciafaloni, D. Colferai, G. P. Salam, and A. M. Stasto, Phys. Lett. B **541**, 314 (2002).
[72] A. H. Mueller and G. P. Salam, Nucl. Phys. **B475**, 293 (1996).
[73] A. H. Mueller and A. I. Shoshi, Nucl. Phys. **B692**, 175 (2004).
[74] A. H. Mueller and S. Munier, Phys. Rev. D **81**, 105014 (2010).